



Challenges in synthesis of heterostructures

Journal:	<i>Journal of Materials Chemistry C</i>
Manuscript ID	TC-REV-01-2022-000324.R1
Article Type:	Review Article
Date Submitted by the Author:	16-Mar-2022
Complete List of Authors:	Miller, Aaron; University of Oregon, Chemistry & Biochemistry Johnson, David; University of Oregon, Chemistry & Biochemistry

REVIEW

Challenges in synthesis of heterostructures

Aaron M. Miller^a and David C. Johnson^aReceived 00th January 2022,
Accepted 00th February 2022

DOI: 10.1039/x0xx00000x

Developing the ability to reproducibly prepare materials drives the advancement of human technology. Trends in historical advances and extrapolation of current technologies suggests that the next logical step is developing the ability to control structure and composition at near atomic scales in device manufacturing to take advantage of emergent properties discovered in 2D materials and heterostructures. This article reviews a subset of synthetic approaches used to prepare heterostructures, outlining key reaction steps, and how experimental parameters are used to control which product forms. The positive attributes of each synthesis approach is discussed along with some of their limitations. The elemental reactant (MER) approach is discussed in more depth.

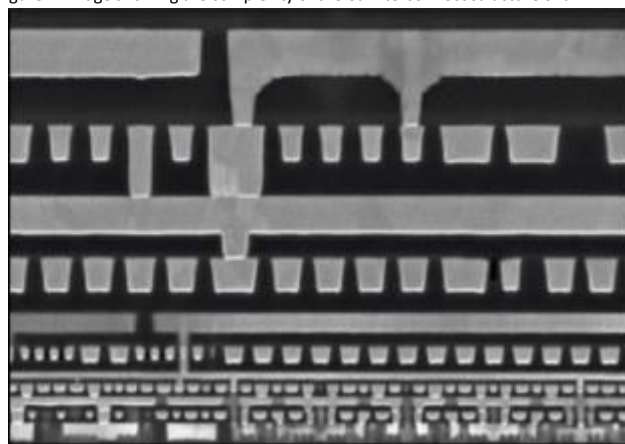
1. Introduction

Materials discovery is a significant factor driving the development of new technology. The history of humanity is even discussed through the lens of materials discoveries, with eras named after materials that enabled significant advances or cultural shifts. As technology has improved, it has done so in part by increasing the fundamental understanding of material properties at ever decreasing scales and with increasing precision. Indeed, it has only been about a century since the mathematical frameworks describing quantum mechanics were theorized.^{1,2} While modern devices based on silicon (Si) exploit our understanding of bulk material transport physics, there are still many remaining unanswered questions and poorly investigated physical phenomena in the quantum regime.

In today's era, the Silicon Age, electronic devices built on Si have become ubiquitous in everyday life. Reducing feature size to increase device density of integrated circuits and computational speed has been a major driver for Si technology. Current chip designs have feature sizes at the nanometer scale and material properties are beginning to no longer scale with dimensions due to quantum effects and reduced material dimensionality.³ The increased complexity of today's chips is evident in the microscope image shown in Figure 1, which depicts a typical Cu interconnect structure. As feature size continues to decrease, more and more elements are also being used to tailor properties. As feature size continues to decrease, it will be necessary to develop a more complete understanding of the interactions between different materials at interfaces. Device properties will no longer predictably scale with size due to quantum effects and emergent properties from the interactions occurring at interfaces.

It seems likely that the next era of human materials use will involve manipulating materials at ever smaller scales, eventually being limited by the size of the constituent material's unit cells. In 2004, Novoselov and Geim observed that the

Figure 1. Image showing the complexity of the Cu interconnect structure of a 14 nm logic



integrated circuit featuring FinFET's and air-gapped interconnect. © 2014 IEEE. Reprinted, with permission, from 54.

properties of graphite changed significantly when it is a monolayer thick.⁴ Monolayer thick graphite – now called graphene – has a gapless Fermi surface due to the removal of interlayer interactions between adjacent layers, which results in graphene's emergent properties.^{5,6} These discoveries were made possible by the 'scotch tape' synthesis method and the discovery that layer thickness could be observed optically due to an interference effect when the resulting flakes were deposited on a thin layer of SiO₂.^{7,8} Energetic research efforts resulted in subsequent reports of emergent properties in other two-dimensional (2D) materials, along with the discovery that the emergent properties had a significant dependence on the identity of the substrate the 2D material was grown on.^{9–15} Theorists have been able to predict unusual emergent properties for specific arrangements of layers, including new quantum states created by the interaction of the properties of different constituent layers.^{16–21} Using exquisite micromechanical manipulation of cleaved flakes, assembly of different 2D layers into stacked heterostructures has been successfully used to verify several of these theoretical

^a Department of Chemistry & Biochemistry, University of Oregon, Eugene, OR.

REVIEW

predictions and construct basic electronic devices.^{22–26} 2D layers can be stacked like bricks in different sequences, as shown in Figure 2, to create desired properties. These discoveries launched the field of 2D materials, as researchers explore tuning the interactions between 2D layers by stacking them in different orders and thickness to form metastable heterostructures.²⁷

The rapid growth of research focused on 2D materials results from the fundamental differences between heterostructures and composites. While both contain regions with distinctly different structures and properties, the properties of composite materials typically scale from those found in the bulk phases, although interfaces can increasingly impact properties as the size of the structural domains decrease to the nanoscale. In heterostructures, properties and/or structures distinct from those found in the bulk constituents arise as the thickness of constituent layers are reduced to monolayers. The lack of adjacent layers changes the band structure of monolayers, causing changes in electronic properties. For example, graphene has a gapless Fermi surface,²⁸ monolayers of semiconducting dichalcogenides have a direct band gap rather than the indirect band gaps found in the bulk compounds,^{29–31} and the charge density wave onset temperature and structure of VSe₂ differ from that found in the bulk.^{32–35} The changes in electronic bonding as thickness is reduced to a single unit cell can also result in structural changes. These structural distortions are typically small in layers exfoliated from 2D solids with very anisotropic bonding, as the perturbation of removing adjacent layers bound via van der Waals bonding is small. The distortions can be much larger if the constituent's bulk structure is less anisotropic. For example, a bilayer of PbSe has a 0.4 Å puckering compared to the bulk structure.³⁶ Charge transfer between adjacent layers can also cause significant structural changes. For example, a charge donating layer next to MoSe₂ can cause a 1T polytype to form.^{37–39}

Since layer properties vary with thickness and identity of adjacent layers, the building-block approach of stacking 2D layers in specific sequences to form van der Waals heterostructures results in an inexhaustible number of different target materials/heterostructures.^{40–43} For example, consider an 8 layer heterostructure constructed from 4 layers of 1T-TiSe₂ and 4 layers of PbSe (total thickness of ~5 nm). One could construct 6 different heterostructures by varying the stacking sequences of the 4 PbSe and four TiSe₂ layers – all having the

same size repeating unit and the same overall composition. The simplest case would be a 4 layer thick block of TiSe₂ stacked sequentially with a 4 layer thick block of PbSe. Five other possible heterostructures can be created by varying the order in which the TiSe₂ and PbSe layers are stacked. Representative HAADF-STEM image cross-sections of these isomeric heterostructures are shown in Figure 3.⁴⁰ An experimental approach needs to be developed where varying experimental parameters enables the stacking sequence and the number of constituent layers to be freely varied to optimize the properties of the resulting devices.

There typically are large differences between the strength of bonding within 2D layers versus between 2D layers. The prototypical 2D layer – graphene – illustrates this case. The carbon atoms in graphene layers are strongly covalently bonded to one another. Monolayers of graphene can be exfoliated from graphite because there is only bonding between the layers in graphite. The strong in plane bonding found in 2D layers that can be exfoliated from the bulk typically make them chemically stable. When on a substrate or adjacent to another 2D layer there will be chemical interactions in addition to van der Waals forces because the wavefunctions of both will overlap, often to a significant degree. The difference in chemical composition and structure between the layers will also result in a chemical potential difference. Charge transfer will occur to equalize the chemical potential. These additional interactions can be surprisingly strong, as evidence by the occurrence of minerals with misfit layer structures that can contain interwoven monolayers of two different constituent layers. Like artificially stacked monolayers, these minerals and analogous thermodynamically stable synthesized compounds consist of two structurally distinct layers whose lattices do not structurally match, resulting in an incommensurate structural mismatch. An excellent review by Wieggers details the structure and properties of misfit layer compounds containing transition metal dichalcogenide constituent layers.^{44,45} Despite the structural misfit, the bonding between the constituent layers is strong enough to make them chemically stable with respect to mixtures of the constituent compounds. In some of these compounds significant charge transfer between constituent layers results in strong ionic bonding between layers, for example (LaS)_{1.2}(CrS₂), where the subscript 1.2 results from the lattice misfit between the in plane unit cell of the distorted rock salt structured LaS layer and the distorted hexagonal CrS₂ dichalcogenide layer. The LaS layer is positively charged while

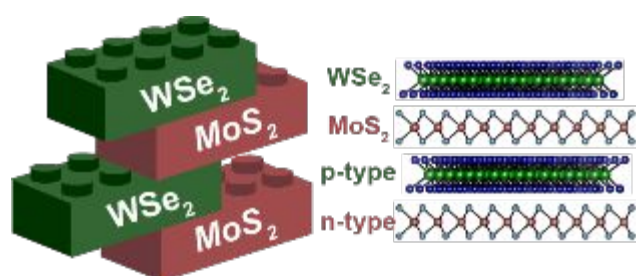


Figure 2. The ability to prepare heterostructures by stacking 2D layers in designed sequences enables preparation of 2D electronic devices, such as this hypothetical stack of alternating *p*- and *n*-type semiconducting layers.

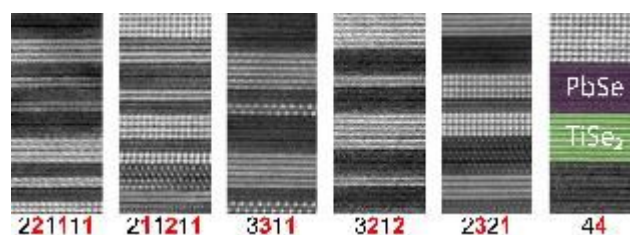


Figure 3. Representative HAADF-STEM images of six of the possible “isomer” heterostructures constructed from a unit cell consisting of various layering schemes of four layers of 1T-TiSe₂ and four layers of PbSe. Because HAADF-STEM intensity increases with atomic number, the PbSe layers are significantly brighter than the TiSe₂ layers.

the CrS_2 layer is negatively charged.⁴⁶ The origin of the strong interlayer interaction is less obvious in other misfit layer compounds, for example $(\text{SnS})_{1.17}\text{NbS}_2$. As the variety of heterostructures that are prepared expands, the range of interlayer interactions will expand.

Historically, many material discoveries have occurred via serendipity.⁴⁷ This is largely because traditional synthesis approaches typically make only the most thermodynamically stable product, which may or may not be the targeted compound. Despite its successes and the discovery of many unpredicted structures and phenomena, these approaches are quite inefficient, especially when targeting a specific structure. Traditional organic synthesis, with its toolbox of well-known reactions and the ability to retrosynthetically design a sequence of steps to systematically assemble a complex structure, is perhaps the most developed synthetic chemistry field. However, even in organic synthesis, the crystal structure of the resulting compound cannot be experimentally controlled. In an ideal world, materials scientists would be able to predict the existence of new compounds with desired properties, including metastable phases, and synthetic approaches would be available to make targeted compounds. While this review focuses on approaches to make targeted heterostructures, there is a broader need for synthetic advances. In the last decade, significant advances have been made in predicting possible new phases through targeted programs such as NIST's Materials Genome Initiative, the Materials Project, and other related coordinated efforts.^{48,49} Of the thousands of predicted compounds, only a small percentage have been made experimentally.⁵⁰ While this may be partially due to the accuracy of the calculations, synthesis limitations also play a significant role.

The remainder of this review focuses on synthetic approaches to heterostructures, briefly describing the reaction pathway(s) typically involved in these synthetic approaches. Since most heterostructures are metastable, they cannot be prepared as bulk compounds by direct, high temperature reaction of the elements and it will be challenging to prepare targeted metastable compounds as films on substrates using flux-based synthetic methods. A short summary of various solid-state synthesis techniques used to grow crystals of thermodynamically stable heterostructures introduces basic concepts. We then discuss vapor phase deposition approaches, which have classically been used to prepare thin films and superlattices, showing how the rate limiting steps in crystal formation can be controlled by experimental parameters. Micromechanical assembly is discussed next, with a focus on more recent advances that may enable wafer scale. We discuss molecular beam epitaxy (MBE), where substrate structure and reacting fluxes are controlled to define the structure and control orientation thickness of constituent layers in metastable superlattice structures, traditionally of constituents with 3D structures. The final part of this review focuses on a more extensive discussion of the modulated elemental reactant growth technique, a newer alternative approach to heterostructure synthesis that involves nanostructured precursors.

2. Direct Reaction of Elements and/or Compounds

The direct reaction of elements and/or binary compounds to form products is a classic solid-state synthesis technique. Because of the non-uniform initial distribution of each element and the different diffusion rates of elements in the different reactants, a variety of local concentration gradients and intermediate compounds develop during these reactions. The reaction typically contains one or more reaction pathways that may involve multiple intermediate compounds. Since diffusion rates in solids are small, it is necessary to increase diffusion rates and/or decrease diffusion distances to obtain reasonably fast reaction rates. The most common approach uses high temperatures to overcome the small diffusion rates and large diffusion distances necessary to form the desired product from the initial reaction mixture. While increasing temperature significantly increases diffusion rates, the resulting composition gradients at interfaces also result in the formation of many of the compounds in the relevant phase diagram as reaction intermediates. The final state is typically the thermodynamically stable mixture of compounds expected from the appropriate phase diagram.

For example, consider the synthesis of misfit layer compound (MLC) $(\text{PbSe})_{1.18}(\text{TiSe}_2)_2$ from the direct reaction of elemental Pb, Ti, and Se, as shown in Figure 4.⁵¹ Typical conditions for traditional synthesis reactions involve mixing stoichiometric amounts of each element in an evacuated quartz ampule and raising the temperature slowly before heating to high temperatures for a week or more. Due to the relatively large differences in melting points of the elements, Se melts and reacts with the surfaces of the Pb and Ti while temperature is being raised. While intuition might predict the most metal-rich phase on the relevant phase diagram would form first.

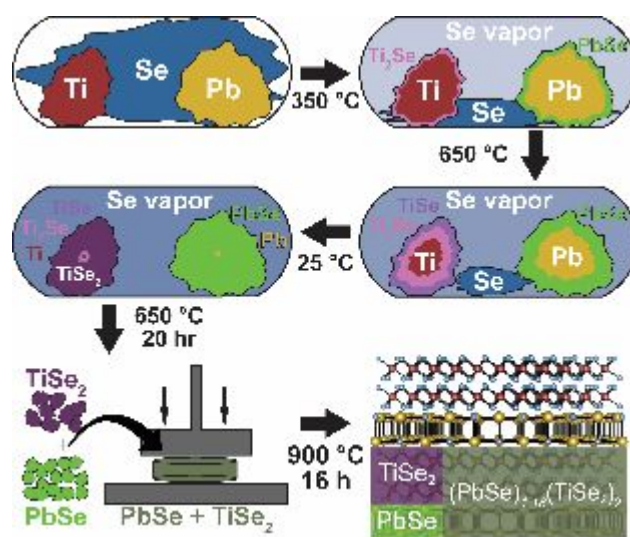


Figure 4. Schematic depiction of the reaction of elements Pb, Ti, and Se to form binary intermediates PbSe and TiSe_2 , and ternary product and misfit layered compound, $(\text{PbSe})_{1.18}(\text{TiSe}_2)_2$.⁶⁴ The direct reaction of elements results in nucleation based on the local composition at that moment in time – here we assume TiSe and Ti_2Se will be the first to form. Since compositions exist from 0 to 100% of each element, there is no control over the reaction pathway.

REVIEW

Journal of Materials Chemistry C

However, the compound that forms first will be the phase with the lowest energy barrier to nucleation. The literature suggests that in this case, the metal rich phase, Ti_2Se is the first Ti-Se-containing phase to nucleate and PbSe is first to form on the surface of the Pb.⁵² The amount of each of these compounds will increase with time as diffusion of elements through the surface product layers occurs. As heat is continually applied to the reaction mixture, the longer diffusion paths through the increasingly thick surface layers decrease the reaction rates. At some point, the targeted thermodynamically stable ternary MLC may nucleate and grow in the composition gradients, but the growth rate is slow due to the low diffusion rates of the elements in the intermediates formed, PbSe and $TiSe_2$. Grinding the intermediate reaction mixture and pressing a dense pellet of the resulting powder decreases the diffusion distances, which speeds the formation of the thermodynamically stable MLC.

While this approach is effective at synthesizing MLC's and other thermodynamically stable heterostructures, it lacks any control over the reaction pathway and thermodynamically unstable compounds cannot be prepared using this approach. Repeated grinding or ball-milling the reaction charge is one of the simplest approaches that can be used to reduce the average particle size by breaking up the product forming on the surfaces of each particle. This decreases the time it takes to convert the reaction mixture to products. While this can be effective at reducing diffusion distances by orders of magnitude ($\sim mm$ to $\sim \mu m$ or smaller), multiple grindings can be required. Researchers often turn to other synthetic techniques that are less diffusion limited, especially when single crystals are desired.

3. Fluid-assisted Synthesis Techniques

Another strategy to bypass large diffusion distances is to use a fluid phase to significantly increase diffusion rates, which can both lower reaction temperatures and decrease reaction times. The large increase in diffusion rates relative to those found in solids allows for facile transport and mixing of reactants across the fluid portion of the reaction mixture. The choice of fluid is diverse and goes by a plethora of different identities and names, including solvent, melt, mineralizer, eutectic melt, flux, or reactive flux. When forming a solid crystal from a fluid phase, nucleation is typically the rate limiting step.⁵³ The compound with the lowest activation energy to nucleate will form, not necessarily the compound that is most thermodynamically stable. Having nucleation be the rate limiting step in crystal formation has the added advantage of allowing for the direct formation of ternary phases without proceeding through binary intermediates, providing the ternary phase is the easiest to nucleate.

The reaction pathway in a fluid-based synthesis can be quite complex. There are basically two strategies used by researchers. Either the initial reaction mixture can be heated to a high enough temperature for long enough time that all the reactants dissolve in the fluid or researchers will focus their search for

compounds formed during the initial heating, before all the reactants dissolve. In both cases, crystal growth will deplete the fluid of the solvated species contained in the compound, potentially causing significant differences in the speciation of the fluid phase. In the case of a heterogeneous reaction mixture of a fluid and undissolved reactants, nucleation and growth impacts the rate that reactants dissolve. *In-situ* studies of melts frequently report nucleation of kinetically stable compounds at short times. A sequence of nucleation events as the reaction proceeds results in a series of new compounds forming, which can cause those previously formed to dissolve.^{54–58} Figure 5 depicts a schematic of this sequence of phase formation.

There is unfortunately little systematic understanding of speciation and how speciation varies with time, composition, or temperature in fluid-assisted solid-state synthesis. While recent *in-situ* total scattering and diffraction experiments have provided insights to the evolution of structure in fluids during reactions and on the sequence of crystalline phases that form in specific systems, it is still not straightforward to predict how reaction parameters can be manipulated to achieve a specific product.⁵⁹ Recent advances in machine learning have provided encouraging insights into understanding how varying the reaction parameters affect the observed reaction pathway, and this approach may be particularly useful for reactions in fluids, which contain many coupled parameters (including the amounts of undissolved reactants and products, the concentration of different species in solution, the reaction time and temperature) that all impact the resulting nucleation and crystal growth processes.⁶⁰

Relative to the direct reaction of elements, the added experimental parameters in fluid-assisted synthesis provide more degrees of freedom to steer the reaction towards desired products. Researchers have used chemical insight to prepare homologous series of related compounds by tuning reaction parameters.⁶¹

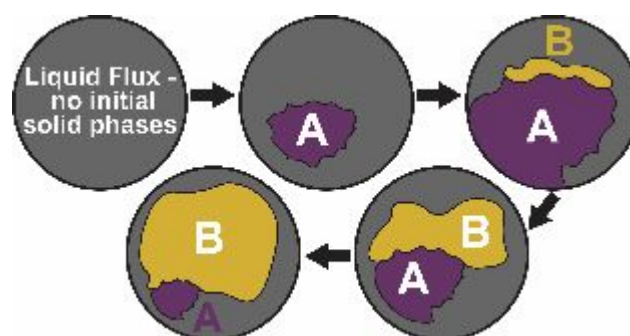


Figure 5. Schematic depiction of the evolution of the nucleation of crystalline phases during the cooling of a fluid-assisted synthesis reaction. The first phase to nucleate as the reaction is cooled to create supersaturation is simply the easiest to nucleate from the liquid (Phase A), given the species in the fluid and their concentrations. This phase is not necessarily the most thermodynamically stable phase. Growth of the first phase changes the speciation of the flux, potentially resulting in nucleation and growth of a subsequent phase (Phase B). As Phase B grows, it depletes the flux of species, which may result in Phase A dissolving.

4. Chemical vapor transport (CVT)

Chemical vapor transport (CVT) reactions are a common approach used by researchers when growing bulk crystals of transition metal dichalcogenides (TMD's) and other layered materials.⁶² As shown in Figure 7, reactants are typically sealed in an evacuated quartz ampule with a transport agent (or mineralizer) and placed in a temperature gradient. CVT reactions involve three basic steps: reaction of the transport agent with the material to be transported to form a vapor phase compound, transport of this compound to the other end of the ampule, and the decomposition of this compound as the product forms.⁶² The transport agent released by the decomposition of the transport compound returns to the reactant side of the vessel to react again. To nucleate the desired phase, the ampule must become super-saturated with the vapor species needed to form the product. Heterogeneous nucleation typically occurs at the surface of the substrate or on the ampule walls.⁶³ Once a crystal forms, it is easier to grow the crystal than nucleate a second one. The example shown in Figure 6 involves a reaction to form MoS₂, a well-studied 2D TMD.⁶⁴ In this example, elemental Mo reacts with the chosen transport agent, I₂, at the hot end of the temperature gradient producing a vapor phase mixture of MoI_x and S_n intermediate species. These intermediate species react at the other end of the temperature gradient, known as the deposition zone, forming MoS₂ crystals and reforming the I₂ transport agent.

The change in the Gibbs free energy as the transport agent reacts with the material to be transported can be used to identify potential transport agents. If the reaction of the transport agent with the material to be transported has a very large negative ΔG and hence a very large ($>10^4$) equilibrium constant, the gas phase product will not readily decompose at the other end of the reaction vessel. If the reaction of the transport agent with the material to be transported has a very small ($<10^{-4}$) equilibrium constant, then the concentration of the vapor phase species will be very small. Either of these thermodynamic conditions make transport of the reactant very inefficient and impractical.⁶⁵ Finding a suitable transport agent becomes more difficult when attempting to synthesize compounds containing more than one metal constituent, as the above constraints must be satisfied for all species that can be formed by reaction of the transport agent with non-volatile

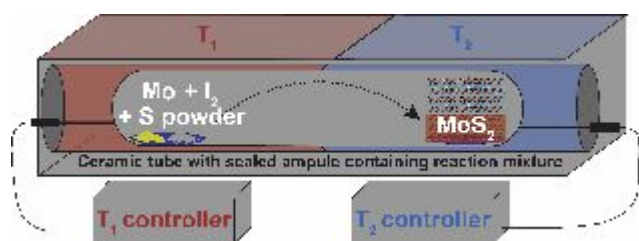


Figure 6. Schematic depiction of the CVT synthesis of MoS₂. A stoichiometric mixture of Mo + S powders and the chosen transport agent, I₂, are sealed inside an evacuated quartz ampule. The ampule is placed across a well-defined temperature gradient within a multi-zone tube furnace. The temperature gradient is chosen such that the reaction and vapor-phase transport of the reactants to the other side of the ampule, where they are deposited as products, is thermodynamically favorable.⁶⁴

elements. Recently it was demonstrated that μm^2 area MoS₂ monolayer crystals and few-layer ReS₂, MoSe₂, and TiSe₂ could be grown using CVT by designing reaction vessels with constrictions.⁶⁴ This is a very encouraging breakthrough, showing that with sufficient control over and understanding of how experimental parameters affect the chemistry involved, the reaction pathway for CVT-based growth can be controlled to obtain monolayer crystals. To the best of our knowledge, however, growing a unique second material as a monolayer on top of a first monolayer has yet to be demonstrated via a closed system CVT reaction.

5. Chemical vapor deposition (CVD)

Chemical vapor deposition (CVD) reactions are like CVT reactions, but epitaxial substrates are typically used to reduce the activation energy for heterogeneous nucleation of a targeted structure. The ability to individually vary the partial pressure of species by varying the source temperatures allows control over the relative concentration of gas phase species in the growth zone to achieve conditions for nucleation and growth. By controlling deposition time, one can control the thickness of the resulting film.⁶⁶ Typically, CVD synthesis begins with solid or gaseous precursors which are heated to generate a partial pressure of each reactant in a carrier gas. The carrier gas containing the precursors is flowed through the reaction chamber. When the precursors impinge on the heated substrate, they decompose and the resulting species react to form the product, as shown in Figure 7.

An important feature of CVD reactions is the significant number of experimental parameters available to tune product formation relative to traditional solid-state synthesis. Perhaps the most critical parameter to control is the residency time of each reactant in the reacting zone. This is done by controlling

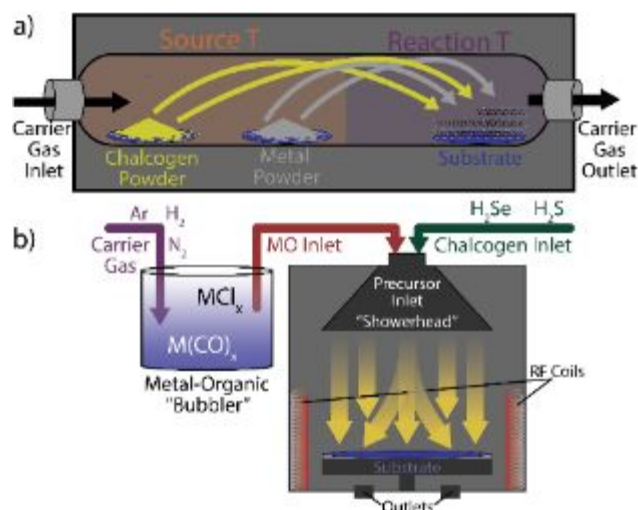


Figure 7. Schematic depictions of two types of CVD reactors. a) Powder-based chemical vapor deposition (CVD), in which powdered sources are used to generate the vapor, which is transported via carrier gas to the substrate. b) Metal-organic CVD, in which the carrier gas is bubbled through a metal-organic-containing solution prior to being injected into the reactor. Both experimental setups are open systems, with the carrier gas and remaining reactants continually removed from the reaction vessel. Adapted from ⁶⁷.

the partial pressures of each reactant in the carrier gas at the substrate, which is typically done by setting the temperature of the sources of the precursors.⁶⁸ The flow of a carrier gas controls the residency time of each reactant in the reacting zone. The carrier gas is typically an inert gas such as nitrogen or a noble gas but occasionally hydrogen or another reactive gas is mixed in to help decompose precursors at lower temperatures. The carrier gas, its temperature, and the partial pressures of the reactants, all affect the number of collisions between reactants, the gas phase reaction between them and the number of reactant species impacting the substrate surface. The ratio η/η_0 affects the initial incubation time observed prior to regular growth for many CVD reaction,⁶⁹ which is probably related to the initial nucleation of the target structure. The substrate temperature controls the decomposition rates of the precursors that impact and adsorb, the surface mobility of the resulting species and their residency time, and the nucleation rate and growth rate of forming solids.

The manipulation of the experimental parameters has significant effects on the observed growth mechanism of the deposited material. CVD growth typically begins with an incubation time prior to a period of regular growth. During the incubation period, the concentration of species on the substrate surface increases until supersaturation is reached, and nucleation occurs. Differences in nucleation energy can result in the formation of metastable compounds, which is typically encouraged by choosing substrates with an epitaxial relationship with the metastable phase. High temperatures result in thermodynamic-controlled processes, while low temperatures result in kinetic-controlled processes.⁷⁰ Once nucleation occurs, growth rate is limited either by the rate of the chemical reaction or by the rate of material reaching the surface. A high concentration of reactants in the vapor phase and low substrate temperatures lead to crystal growth being limited by the rate of the chemical reaction. A low concentration of reactants in the vapor phase and high substrate temperatures result in a mass-transport limited growth mechanism.

There is often a balancing act between using a sufficiently high substrate temperature to promote crystal growth but a low enough temperature to avoid desorption of reacting species from the surface. For example, in the growth of dichalcogenides reaction rates initially increase with temperature before decreasing as concentration of chalcogen on the substrate surface decreases due to its significantly higher vapor pressure than the other reactants. Since many TMD's lose chalcogen atoms when heated to high temperatures, the substrate temperatures must remain low enough to inhibit the formation of chalcogen vacancies. The number of chalcogen vacancies can dominate the properties of the resulting film.⁷¹

Three distinct growth modes have been observed in CVD growth, depending on reaction conditions: 2D layer-by-layer growth, also known as Frank-van der Merwe (FM) growth, 3D island-based growth, known as Volmer-Weber (VW) growth, and Stanski-Krastanow (SK) growth, which is a combination of the first two, involving formation of a few 2D layers followed by

3D island formation.^{69,72–74} FM growth occurs when the interaction between the incident reactants and the substrate is greater than that between the incident reactants and itself ($\eta < \eta_0$), resulting in preferential growth of each complete layer before nucleation of the next layer.⁷⁵ VW growth occurs when the interaction between the incident reactants and the substrate is weaker than the interaction between the incident reactants and itself, which causes mostly vertical growth of the nucleated islands, typically resulting in films with very rough surfaces.⁷⁶ SK growth is a mixed growth mode that occurs when the interaction between the incident reactants and the substrate is about equal to that between the incident reactants and itself, resulting in competition between island nucleation and layer growth.⁷⁷ None of these growth mode models account for the initial incubation time.⁷⁴ While strides have been made to modify the growth models to account for these other involved processes, a complete understanding of CVD reactions has remained elusive.⁶⁹

There are still significant challenges to using CVD reactions to synthesize metastable 2D films and heterostructures. One challenge is exactly determining when a layer's growth is complete, because incubation times vary and are sensitive to experimental conditions. When growing multiple constituents, one must determine exactly when layer growth is completed, such that growth of the first material can be halted prior to switching sources and growth of the second material. This requires reproducibly controlling two different incubation periods that may require different reaction conditions. In an encouraging breakthrough, Zheng *et al.* used a sequential two-step CVD method to grow a monolayer PbI_2 on monolayer WS_2 and WSe_2 .⁷⁸ This was enabled by the much lower growth temperature of PbI_2 relative to WSe_2 and WS_2 (400 °C vs. 1050 °C). These different growth temperatures, however, prevents the growth of WSe_2 or WS_2 on PbI_2 .

6. Micromechanical assembly

The mechanical assembly processes for synthesis of heterostructures is conceptually straightforward, involving the sequential stacking of 2D layers in the same way that one might stack bricks or Lego blocks, as depicted earlier in Figure 2. The steps involved in mechanical assembly consist of the initial growth of films or crystals that provide the source of the 2D layers, the exfoliation of the 2D layer of desired thickness from the crystal or substrate, the transfer of the layer to the growing assembly, and the removal of the substrate used to transfer the layer. One of the first reports of high-quality micromechanically assembly utilized small flakes of mechanically exfoliated mono- and bilayer graphene to make simple devices on single-crystal h-BN substrates.⁷⁹ The ability to prepare targeted structures with designed architectures in such a straight forward manner has resulted in literally thousands of papers published further optimizing each of the steps involved or using an assembly process to make targeted heterostructures. We will not attempt to comprehensively review all this literature, as excellent reviews on targeted aspects already exist,^{80–82} but will highlight what we

believe were key synthesis advances as the size of the assembled structures increase towards wafer scale.

Major advances and remaining challenges in growing 2D materials over large areas were discussed earlier in this article. It is now possible to prepare large area, monolayer thick films of many 2D materials with near complete coverage of the substrate.^{83,84} Since this technique allows one to individually prepare each layer, ensuring it is the correct thickness and composition, the challenges in finding compatible growth conditions to sequentially deposit different materials is avoided altogether. However, one challenge in developing growth techniques for a new 2D material is finding a substrate that enables crystallographically aligned growth, while also permitting the film to be exfoliated as a large area film from the substrate. It is necessary to optimize the CVD growth of the 2D layers to generate surface properties that enable the 2D layers to be cleanly isolated from substrates they were grown on without the use of any etchants or solvents.

The exfoliation of 2D layers from both crystals and growth substrates has undergone significant advances since Frindt first used tape to exfoliate NbSe₂ crystals to measure the effect of sample thickness on superconductivity.⁸⁵ Early methods typically used an adhesive layer, which needed to have a stronger adhesion with the material being cleaved than the interaction of the material with either the neighboring layers of itself in a crystal or to the substrate if grown as a film. An alternative approach to create large amounts of monolayer material is chemical exfoliation, in which ions and/or solvent intercalate between the 2D layers resulting in free floating solvated layers in solution.^{86–88} Like mechanical exfoliation, the solvation energy of the solvated layers must be larger than bonding between the layers in the 2D crystal for this approach to be successful. It is often challenging to completely remove the adhesive or solvent from the 2D layer when they are being mechanically stacked via either of these approaches. One successful approach to isolate 2D layers of CVD grown films is to spin-coat the grown film with an adhesive polymer film, which is then mechanically peeled from the growth substrate using a thermal release tape.⁸⁹

To get around organic contamination, gold-assisted exfoliation methods were developed.^{90–92} Ultrasoother gold layers result in a significant degree of charge transfer between the monolayer being transferred and the gold layer as the chemical potentials are equalized on contact, resulting in a bond to the gold that is stronger than the van der Waals forces between the 2D layers themselves. While contamination still can occur when removing gold films with chemical solvents in subsequent processing steps, the Au transfer process works for a wide variety of 2D materials.²⁴

Initial micromechanical assembly was done manually on small, cleaved layers from crystals to discover emergent properties and to test theoretical predictions. Approaches were developed that enabled layers to be stacked with control of the rotational angle between the crystal structures of adjacent layers.⁹³ More recently, automated assembly techniques have been developed to improve reproducibility, decrease incorporated material between the 2D layers, and increase

throughput on large area substrates.^{94,95} These advances enable researchers to consistently synthesize wafer-scale heterostructures, which is an essential step towards being able to manufacture devices made from heterostructures.

7. Molecular beam epitaxy (MBE)

Molecular beam epitaxy (MBE) growth is a well-developed and understood technique and is one of the few synthesis techniques able to target and grow metastable materials and superlattices. This ability positions MBE as a potential source of 2D layers that cannot be prepared as bulk compounds or via CVD. MBE is similar to CVD reactions in some respects, but MBE reactions differ by taking place in a high or ultra-high vacuum environment. An advantage of utilizing high-vacuum and ultra-pure sources is the lower occurrence of impurity inclusions from carrier gas molecules or other source impurities, relative to films grown via CVD.⁶⁷ A second advantage is that *in-situ* characterization tools are available to monitor film growth during deposition, including surface-sensitive reflection high-energy electron diffraction (RHEED), quartz crystal deposition monitors (QCM), auger spectroscopy, and scanning tunnelling microscopy (STM).⁶⁷ These analytical tools have enabled researchers to develop and understand the reaction pathways and how and why experimental parameters change growth modes.

MBE involves heating ultra-pure reactant sources with effusion cells and/or electron beam guns to generate “beams” of vaporized reactant, which are co-incident on an actively heated substrate, as shown in Figure 8. The heated substrate allows for significant surface diffusion of the reactants after they impact the substrate, enabling them to find energetically favorable locations such as step edges on the growing surface. Relatively low temperatures can be used, which minimizes the formation of vacancy defects and limits interlayer diffusion to keep interfaces abrupt.

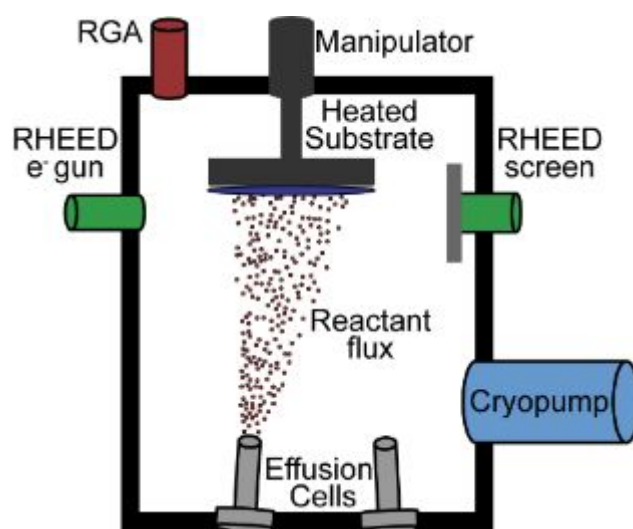


Figure 8. Schematic of MBE reactor, showing effusion cells with a reactant flux incident on the heated substrate, along with *in-situ* RHEED instrument for characterization of film growth during deposition.

MBE exploits the difference in activation energies between surface and bulk diffusion, providing enough thermal energy for adatoms to move and react with already nucleated layers, but not enough for bulk diffusion. By changing the substrate temperature, the observed growth mechanism during deposition can be varied. To target a specific structure, an epitaxial match between the substrate and the targeted product is used to favor nucleation of the targeted structure. When the incident reactants impact the substrate, they interact with the dangling bonds present on the substrate's surface, initially taking on the lattice constant of the substrate.⁹⁶ In practice, the crystal lattices of the chosen substrate and the desired material have lattice parameters that are typically within 5% of one another. If there is a mismatch between the lattice constants of the deposited material and the substrate, increasing strain-induced distortions with thickness result in the formation of dislocation defects.^{97–99} The critical thickness where dislocations occur is dependent on the system, dictated by the extent of the lattice mismatch and the activation barrier to nucleation of the dislocation defect.¹⁰⁰ The presence of periodic dislocation defects in the lattice of the thin film can degrade the electrical performance of devices fabricated from these materials.¹⁰¹

The development of so-called “van der Waal's epitaxy” (VDWE) by Atsushi Koma's group in the late 1980s opened a new regime where epitaxy is no longer a strict requirement for ordered growth. Koma utilized typical MBE growth conditions but used substrates with a lack of dangling bonds on the surface.^{102–105} Koma showed that the materials grown had the lattice parameters of the bulk compounds, not those of the substrate. Large lattice mismatch's of up to 20% or more were possible, because the lattice of the material being grown no longer adapted to the substrate's lattice during the first few layers of growth.¹⁰⁶ VDWE epitaxy has been used to grow transition metal chalcogenides, TMD's, and other 2D materials of interest,^{107–110} and to grow TMD heterostructures and topologically insulating materials, such as Bi₂Te₃.^{111–113}

The growth of large domain size mono- or few-layer transition metal dichalcogenide films via MBE, however, has been surprisingly difficult. For MBE-grown transition metal dichalcogenides (TMD's), typical growth conditions (<500 °C, with a ~20:1 chalcogen:metal flux ratio) result in a relatively high nucleation rate.^{114,115} This leads to a dense distribution of small grains in the resulting film, with the high density of grain boundaries limiting electrical performance of devices fabricated with these materials. As of 2017, the largest reported grain sizes for an MBE-grown TMD were relatively small, around 250 nm, observed in separate reports of NbSe₂ and WSe₂ films.^{116,117} In the WSe₂ case, the authors report that the grain size significantly increased with the substrate growth temperature, although the nucleation density was still so high that the overall maximum grain size was restricted due to space considerations on the substrate.¹¹⁷ To achieve larger grain sizes, surface diffusion rates must be increased while the nucleation rates must be decreased, which is challenging given that both diffusion and nucleation rates increase with temperature.⁹⁶ When using high substrate temperatures, sticking coefficients

are much lower relative to those observed at lower temperatures. This results in a lower density of surface adsorbed atoms (adatoms) at high temperatures leading to a lower probability of the formation of nuclei of critical size.

Hinkle's group recently showed that applying the above concepts result in over an order of magnitude increase in the observed grain sizes for MBE-grown WSe₂ films.¹¹⁴ The challenge in applying these ideas to TMD growth, however, is that chalcogen adatoms have a significantly increased likelihood of desorbing, due to their much higher vapor pressure relative to metal adatoms. Consequently, the disparity in reactant fluxes needed to form stoichiometric dichalcogenides is closer to 1000:1 chalcogen:metal. The high substrate growth temperatures also result in significantly slower growth rates (around 0.05 monolayer/hour) due to the increase in adatom desorption. While the much slower growth rate observed at high growth temperatures make it unsuitable for industrial-scale production of these materials, it does make it easier to terminate growth with a completed layer. It was recently shown that using a shutter to interrupt the metal beam at regular intervals during MBE growth of TMD's, reduces the probability of metal-metal adatom interactions during deposition and allows more time for the chalcogen reactants to react and bond with adsorbed metal atoms. This clever way to increase the effective chalcogen:metal flux ratio resulted in stoichiometric films and was used to prepare the first reported MBE-grown WTe₂ film.^{118,119}

In summary, the layer-by-layer growth enabled by MBE is an extremely powerful tool in the synthesis of metastable materials and heterostructures. However, there are still significant challenges to extending these advances to the growth of heterostructures using MBE. For example, it can be extremely challenging to grow Material A on Material B AND Material B on Material A, due to the large differences in growth conditions required. The ability to prepare 2D layers not found in equilibrium phase diagrams, however, make MBE potentially a key growth technique to supply micromechanical assembly platforms with 2D layers that cannot be obtained via other approaches.^{120–124}

8. Modulated elemental reactants (MER)

MER is the newest of the synthesis approaches outlined in this review, hence we will provide a longer description of this technique. MER is based on the idea that a homogenous, amorphous intermediate is a valuable and general starting point for the synthesis of metastable compounds, as all crystalline compounds will be more thermodynamically stable than the amorphous phase.¹²⁵ Nucleation is the rate limiting step in forming a crystalline solid from an amorphous state, which depends on the local concentration and on the prior thermal history of the sample. To nucleate a compound with a stoichiometry different from the composition of the amorphous phase, diffusion needs to occur. Since diffusion rates are low in solids, the nucleation of a compound with stoichiometry close to that of the amorphous phase is favored.

A challenge in using the amorphous state as a reaction intermediate was finding a general experimental approach to prepare amorphous alloys of controlled composition. One solution to this challenge was discovered in the early 1980's, when W. L. Johnson's group showed that amorphous metals can be formed by heating crystalline metal foils at low temperatures. The formation of the amorphous alloy is driven by the large enthalpy of mixing.^{126–128} The D. C. Johnson group showed that if the thicknesses of reactant layers are below a critical thickness, an amorphous phase forms before any crystalline phases in a wide variety of different systems.^{129–131} This group also showed that the composition of the amorphous intermediate controls which compound nucleates first.¹³² Since the activation energy required to nucleate a metastable compound from the amorphous alloy with a composition that corresponds to the stoichiometry of the metastable compound can be smaller than that required to disproportionate and nucleate the more thermodynamically stable mixture of binary compounds, this provided a systematic approach to preparing metastable binary compounds. New metastable binary (FeSb₃, NiSb₃ and RuSb₃)^{133,134} and ternary (Hf_{1-x}Fe₄Sb₁₂, and Y_{1-x}Fe₄Sb₁₂)¹³⁴ antimonide compounds with the skutterudite structure were prepared using this approach, showing the ability to make targeted compounds using amorphous intermediates. W. Bensch's group also used designed precursors to prepare amorphous intermediates to synthesize a number of new metastable binary compounds. His group used an array of *in-situ* experiments to show that forming these metastable compounds was a result of the reaction pathway avoiding more stable compounds.^{135,136} Jansen's group synthesized amorphous precursors by simultaneously depositing the relevant elemental sources onto a liquid-N₂-cooled substrate with compositions matching the stoichiometries of intended phases.^{137,138} They synthesized several novel alkali nitride phases, including Na₃N, and a previously unknown LiBr phase by gently heating the amorphous precursors.^{139,140}

The modulated elemental reactants (MER) approach is an extension of these initial findings, based on the hypothesis that the nanoarchitecture of a precursor (elemental layer thicknesses and the layer sequence) can be used to control the resulting reaction pathway. One of MER's advantages is the large number of parameters available to manipulate reaction pathways.^{141,142}

MER precursors are created by depositing sequences of ultra-thin elemental layers (~3–30 Å thick) designed to minimize the total diffusion distance that the reacting atoms need to travel from their initial positions in the layered precursor to their final positions in the targeted crystalline product. Changing the absolute layer thicknesses while maintaining a constant ratio of reactants per repeated sequence has a significant effect on the observed reaction pathway by changing the time required for interdiffusion, which scales as thickness squared. If the layer thickness is above some critical thickness, nucleation of the binary phase will happen at the layer interfaces prior to the formation of an amorphous intermediate. Below the critical thickness, the layers will

interdiffuse and mix before a nucleation event occurs, forming a homogenous amorphous intermediate. The exact value of the critical thickness for each system is defined by the energy and time required to diffuse each reactant through the surrounding matrix relative to the activation energy and time required to nucleate a crystalline phase. As the absolute layer thickness increases, the time required for diffusion will increase until it becomes larger than that required for nucleation.¹⁴³ The typical total diffusion distance for reacting atoms is nanometers in MER, which is smaller than the ~μm-scale surface diffusion lengths found in CVD and MBE, and much less than the ~mm-scale bulk diffusion lengths present in the direct reaction of the elements. The local composition is another important parameter, which is controlled by the relative layer thicknesses of each element deposited.^{131,144} The activation barrier for nucleating a crystalline compound depends on the local composition. For homogenous amorphous alloys, the lowest nucleation energy is observed for amorphous intermediate compositions that corresponded to the stoichiometry of the compound.¹⁴⁵ This gives MER an advantage over other synthetic techniques when attempting to synthesize phases that are predicted to be kinetically stable, because local compositions are controlled by the design of the precursor. If the reactant contains layers or particles thicker than the critical thickness, composition gradients formed during interdiffusion provide opportunities for a variety of different compounds to nucleate. The goal in designing a MER precursor is to have the nucleation and growth of the intended phase be the fastest way for the system to reduce its free energy.

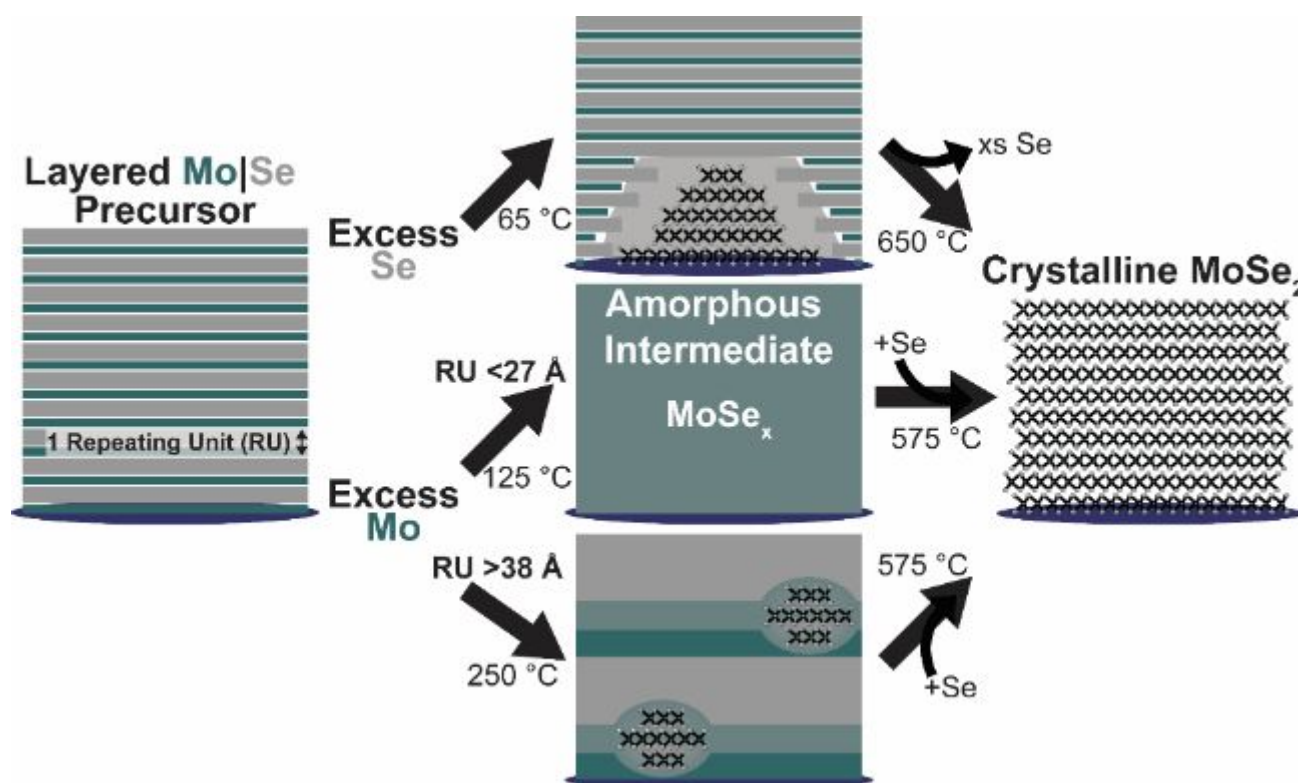


Figure 9. Schematic depiction of two different reaction pathways in the reaction between ultra-thin layers of Mo and Se. If the precursor's composition is Se-rich, small grains of MoSe_2 nucleate during the precursor's deposition. If the precursor is Mo-rich, the thickness of the repeating sequence of layers (Mo|Se) controls the reaction pathway. If the thickness of the deposited Mo|Se sequence is less than 27 \AA , heating the precursor causes interdiffusion of the layers and formation of a homogenous amorphous intermediate state. Further heating crystallizes the majority of the intermediate into the desired MoSe_2 structure, depending on how closely the composition of the intermediate matches the compound's stoichiometry. If the Mo|Se thickness is greater than 38 \AA , nucleation occurs at the interface between Mo and Se layers, trapping any local composition gradients that might be present in the layers. The MoSe_2 grains grow until the trapped local composition gradients have come to equilibrium.

In most systems, the reaction pathway can be controlled by designing precursors with specific interdiffusion lengths and layer sequences to avoid unwanted intermediate crystalline compounds. Low temperatures are sufficient to enable the elements to mix, due to the short diffusion lengths, permitting the initial formation of an amorphous intermediate. What forms from the amorphous intermediate depends on the relative magnitude of nucleation energies of different potential compounds, which is a function of local composition. The reaction between ultrathin layers of Mo and Se, depicted schematically in Figure 9, illustrates the importance of both composition and repeat layer thickness. When Mo and Se are deposited in a metal rich repeating unit that deviates enough from a 1:2 ratio of Mo:Se and has a total thickness of the repeating unit less than 27 \AA , heating the layered precursor at low temperatures ($\sim 125 \text{ }^\circ\text{C}$) causes the interdiffusion of layers and formation of a homogenous amorphous alloy.¹³⁰ Heating the amorphous alloy at $575 \text{ }^\circ\text{C}$ results in the formation of MoSe_2 , indicating that it is the easiest compound to nucleate. If the thickness of the repeating unit is larger than 38 \AA at this composition, nucleation of MoSe_2 occurs at the interface between Mo and Se layers during annealing at $\sim 250 \text{ }^\circ\text{C}$. Depositing bilayers that are Se rich with respect to MoSe_2 results in MoSe_2 nucleating at the interfaces during the deposition for all repeat thicknesses that were studied, which were smaller than 2 nm .⁵² Annealing at higher temperatures results in the growth of MoSe_2 layers perpendicular to the

substrate and the loss of the excess Se at higher annealing temperatures.

In ternary systems, additional experimental parameters can be used to avoid the formation of crystalline binary compounds as reaction intermediates. Addition of a third element to an amorphous intermediate increases the activation barrier to nucleation of possible binary compounds.¹⁴⁶ The layer sequence can also be used to avoid binary compounds as reaction intermediates by controlling the sequence of interdiffusion.¹⁴⁷ If layers are deposited in an A|B|C sequence, all elements are adjacent to one another. If layers are deposited in more complex layer sequences, for example A|B|A|C, one separates the elements B and C to avoid the formation of binary B-C compounds. The ability to control the sequence of interdiffusion to avoid the formation of binary compounds by design of the precursor makes MER an effective approach to use when trying to prepare an unknown ternary phase.

By preparing more complex MER precursors, it is possible to mimic the composition profiles of misfit layer compounds, naturally occurring heterostructures with lattice mismatched constituents. The planar nature of the composition gradients in as deposited MER precursors combined with the low nucleation energy of dichalcogenide compounds often leads to their low temperature nucleation before the deposited layers can mix.^{52,148} In the Ti|Se|Sn|Se precursor shown in Figure 10, monolayers of TiSe_2 form during the deposition, provided the deposited Ti|Se layers each contain the number of atoms

required for a single unit cell of TiSe_2 . The TiSe_2 layers are separated by amorphous SnSe_x . If the deposited Sn|Se layers contained enough Sn and Se to form one unit cell of SnSe , annealing at higher temperatures results in the formation of a $(\text{SnSe})_{1.2}\text{TiSe}_2$ heterostructure.¹⁴⁹ Depositing two Sn|Se layers and one Ti|Te layer results in the formation of the $[(\text{SnSe})_{1.2}]_2(\text{TiSe}_2)_1$ heterostructure.^{150,151} By varying the number of and sequence of deposited Sn|Se and Ti|Se layers in the precursor, MER enables the synthesis of a nearly unlimited number of unique heterostructures, including structural isomers.

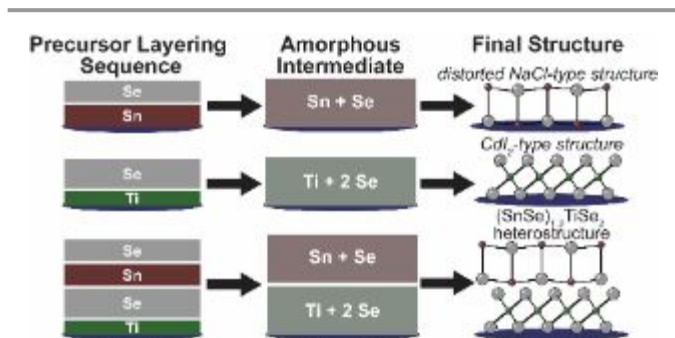


Figure 10. Schematic depiction of two sample layering sequences for deposition of MER precursors used when targeting materials with the distorted NaCl-type structure (top), the CdI_2 -type structure (middle), and a heterostructure combining both layer types.

For example, consider heterostructures containing four layers of compound A and four layers of compound B. There are six different layer sequences that can be constructed containing four layers of A and B that all have the approximately the same c-axis lattice parameter: AAAABBBB, AAABBBAB, AAABBABB, AABBBAAAB, AABBBABAB, AABBBBAB. One can prepare these structural isomers via MER by simply depositing the correct sequence of elemental layers to mimic the composition profiles of these heterostructures. However, as an overall synthetic approach, this results in an extremely large number of potential heterostructures, since the number of possible configurations in the final compound increases rapidly with the number of constituents. Even when limiting selections to those with <20 unique layers in the unit cell, there are nearly 60,000 possible unique heterostructures constructed from only two constituents. With three constituents, this number increases to over 130,000,000; with four constituents, the number of possible structures is more than 35,000,000,000.¹⁵²

MER also enables the synthesis of heterostructures that have no homologs in the systems equilibrium phase diagram. For example, sequentially depositing one Bi|Te bilayer (with a 2 to 3 ratio of Bi to Te) and one Ti|Te bilayer (with a 1 to 2 ratio of Ti to Te) in a MER precursor results in the $(\text{Bi}_2\text{Te}_3)_1(\text{TiTe}_2)_1$ heterostructure.^{153,154} Heterostructures containing MoSe_2 or WSe_2 layers with SnSe , PbSe or BiSe have also been prepared.^{43,155–158} Other heterostructures incorporating novel constituents and combinations of constituents that do not exist on equilibrium phase diagrams have also been reported, based on intergrowths of different layered compounds (including Bi_2Te_3 , TiTe_2 , TiSe_2 , MoSe_2 , VSe_2) and structural fragments of compounds with 3D structures, (including PbSe , SnSe , BiSe , LaSe , and GeSe_2).^{41,144,154,155,159–162} Key to the formation of a

specific heterostructure is controlling the deposition parameters so that the precursors contain the desired ratio of metal atoms to chalcogen atoms (2:3, 1:2, or 1:1) for the Bi_2Te_3 -type, CdI_2 -type structures and MX layers respectively) and the correct number of atoms to form an integer number of crystalline layers of the targeted constituents.

Advances in thin film analytical and characterization techniques have been critical to enable the development of the MER synthesis approach. Low angle x-ray reflectivity quantifies the thickness of repeating layer sequence and infer their compositions.^{163–165} X-ray fluorescence provides a fast and non-destructive technique to determine the absolute number of atoms in each sample.¹⁶⁶ X-ray total scattering techniques and atomic pair distribution function (PDF) analysis can be used to probe the structure of amorphous intermediates.¹⁶⁷ High angle annular dark field scanning transmission electron microscopy (HAADF-STEM) and energy dispersive spectroscopy (STEM-EDS) provide critical atomic scale information about composition, local structure, and morphology.¹⁶⁸ The relative positions and compositions of atomic planes from both HAADF-STEM and STEM-EDS data provide initial structural models for Rietveld structural refinement of specular and in plane diffraction data. When the resulting refinements match the initial model, it indicates that the STEM data is representative of the majority of the sample.

Conclusion

A free energy landscape, first introduced by Schön and Jansen, provides a useful way to discuss the challenges involved in synthesis and the attributes of the different synthetic approaches discussed in this review.^{137,169,170} Consider the schematic of a portion of the free energy surface for the BiSe-NbSe_2 system, shown in Figure 11, which shows some of the kinetically stable and the thermodynamically stable heterostructure with a 1 : 1 ratio of BiSe to TaSe_2 layers in their unit cell. Like lakes that occupy minima in the local topography, each heterostructure is a local free energy minimum in the energy landscape. Differences in the minimum value for each lake reflect differences in the bonding in and between the constituent layers in each heterostructure. The “lake” at the lower left side of the map, labeled **11**, has the lowest “altitude” and hence is the thermodynamic product, $(\text{BiSe})_{1.10}(\text{NbSe}_2)_1$. It has a unit cell containing one BiSe bilayer and one NbSe_2 layer and the strong interaction between the layers make it more stable than heterostructures with thicker layers. The upper right hand lake basin of the map contains 6 isomeric heterostructures containing 4 bilayers of BiSe and 4 layers of NbSe_2 in different sequences, analogous to those discussed in Figure 3, but with different constituents. The lakes in the bottom part of the map represent the two heterostructures that can be created with three layers of BiSe and NbSe_2 layers. Because of the stabilizing electronic interaction between BiSe and NbSe_2 layers, the relative stability of each compound in this system is controlled by the number of interfaces between each constituent layer present in the unit cell. The **11** heterostructure realizes the maximum number of these interactions by layering alternating

BiSe and NbSe₂ layers, making it the most globally stable compound in the system. The depth of the valleys relative to

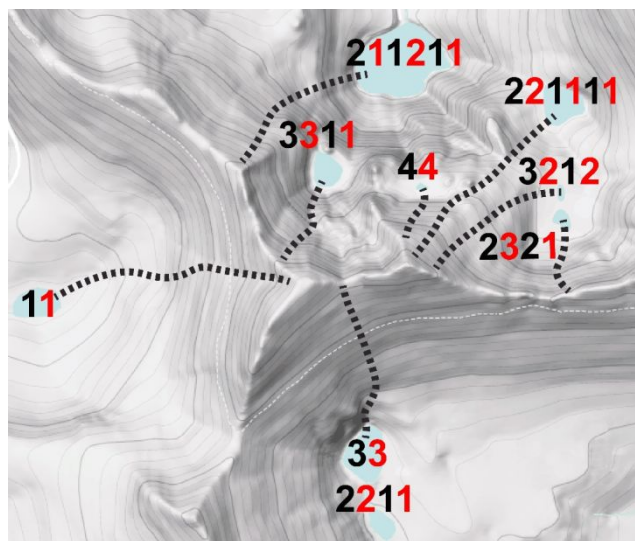


Figure 11. Schematic free energy surface for the PbSe-TiSe₂ system showing some of the possible kinetically stable heterostructures containing an equal number of PbSe and TiSe₂ layers and the thermodynamically stable product (PbSe)_{1.16}(TiSe₂)₁ (labeled 11). By varying the layering sequence or the composition of the MER precursor, one can select a starting position on the energy landscape where the steepest slope results in the precursor evolving into a specific heterostructure. This is analogous to raindrops falling to Earth and flowing down the surrounding topography into a lake.

the saddle points leaving them reflects the kinetic stability of each isomer. While the 6 isomers in the upper right are relatively close in elevation, their relative stability is dictated by the number of interfaces present, 1 for the 44 isomer, 3 for the 3311, 2321, and 3212 isomers, and 5 for the 221111 and 211211 isomers.

To prepare a specific heterostructure, one needs an approach with experimental parameters that can be used to avoid both the other metastable heterostructures and the thermodynamically stable phase at this composition. Traditional high temperature synthesis and vapor transport reactions both yield only (BiSe)_{1.16}(NbSe₂)₁, as they do not have parameters that can be used to control the reaction pathway and composition alone will not work, as all of these heterostructures have the same composition.¹⁷¹ Synthesis using CVD would require shuttling the sample between different experimental conditions to prepare PbSe on TiSe₂ and TiSe₂ on PbSe. Precise deposition control would be required to stop growth at the correct number of completed layers for each constituent. MBE growth would involve the same challenges as CVD, but with added difficulties due to the high vapor pressure of Se at the temperatures required for Ti to have sufficient surface mobility. It may not be possible to find conditions to grow both TiSe₂ on PbSe and PbSe on TiSe₂ using either CVD or MBE growth.

The challenges in synthesizing a specific heterostructure using the MER approach are designing the nanoarchitecture of the precursor (elemental layer thicknesses and the layer sequence) and finding annealing conditions that yield the

desired product. The nanoarchitecture of the precursor determines the initial position on the free energy landscape, which needs to be somewhere within the local valley of the targeted product. Since solid state diffusion rates are small at low temperatures, the initial rearrangements that occur are constrained around the structure defined by the as-deposited precursor. Like water flowing downhill, the steepest slope of the energy landscape controls the pathway that the reaction takes, which is illustrated as dashed lines in Figure 11 for potential starting points. Therefore, it is essential to find a precursor nanoarchitecture that allows the reaction to begin in a spot on the energy landscape where, when annealed, it will flow downhill towards the desired lake. For example, if one wanted to deposit a MER precursor targeting the 211211 isomer, one would need to deposit both the correct number of constituent atoms in each repeating sequence to form 4 total layers of each constituent and the layer sequence needs to be constructed such that the precursor will nucleate and grow the 211211 heterostructure. This is achieved by depositing the correct number of constituent atoms in an order that mimics the composition profile of the desired heterostructure's nanoarchitecture. The annealing conditions must provide sufficient time and thermal energy for the atoms to diffuse and nucleate the targeted structure, but not so much that the precursor moves through a saddle point in the energy landscape into an adjacent valley. Too much time or too high a temperature will cause the precursor to move out of the local minimum, forming a more thermodynamically stable compound. While MER provides access to the desired heterostructure, the trade-off is the lack of control of the rotational order of the constituent layers.

While each of the synthesis methods discussed have different experimentally adjustable parameters that provide some control over the products formed, as summarized in Table 1, further advances are required. Ideally, one would be able to combine the strengths of each, for example the flexibility of fluid-based synthesis approaches, the ability to control what phase nucleates as done in MBE, and ability to prepare single crystals as done using chemical vapor transport, and the ability to define starting parameters as in MER. While the MER approach can prepare many metastable compounds and heterostructures, additional experimental parameters need to be developed to control the structure of what nucleates, both as bulk phases and as individual layers in heterostructures. Controlling nucleation density in MER would also be valuable, as this would provide control of the in-plane grain size of the constituent layers in heterostructures. The Age of Heterostructures will be based on the exciting developments enabled by emergent properties created by controlling structure and composition on the scale of a unit cell.

The development of experimental methods and tools will continue to be an important part of research on heterostructures and devices made using them. The discovery of optical contrast of thin layers on thin layers of SiO₂ distinguishes between layer thicknesses with single layer resolution^{7,8} and the use of x-ray fluorescence to determine the absolute number of atoms per unit area¹⁶⁶ are two examples of

fast and non-destructive techniques that have accelerated discoveries. Advances in focused ion beam¹⁷² and electron microscopy^{173–176} enable detailed atomic level structural, compositional, and vibrational analysis of chosen analytical volumes. The need for enhanced analytical tools will become more important as heterostructure devices enter the development stage. Modern manufacturing, especially of complex devices and integrated circuits, is facilitated by intensive statistical analysis of process data and application of aggressive statistical process control. Analysis tools are the foundation of this approach, both defining baseline conditions and identifying deviations from statistical expectations. The

importance of obtaining data on each manufacturing step will drive the development of new analytical approaches and tools.

Table 1. Summary of synthetic techniques typically used in the synthesis of van der Waal's heterostructures

Synthetic Approach	Typical Conditions	Advantages	Disadvantages
Direct reaction of the elements	open or sealed reaction vessels, temperatures >1000 °C, long synthesis times (days to months)	Easy, low-cost, direct approach to thermodynamically stable compounds	Thermodynamics controls which phase forms, low diffusion rates in solids lead to long synthesis times and/or high reaction temperatures
Fluid-assisted synthesis	in open or sealed reaction vessels, lower temperatures than direct reaction, short synthesis times (seconds to days)	Increased diffusion in fluids allows for shorter synthesis times, additional experimental parameters (composition of fluid) relative to direct reaction of the elements	No control over which phase nucleates first, fluid speciation as a function of time is extremely challenging to determine experimentally, solubility constants not known for most systems, elements from fluid can be incorporated in product
Chemical vapor transport (CVT)	Evacuated ampule filled with reagents and placed across a temperature gradient	Results in growth of single crystals. Few-layer and monolayer growth of films possible with specially designed reaction vessels and appropriate substrates	Can be challenging to find suitable transport agent for systems with multiple metal constituents, suitable substrates may be difficult to find for film growth
Chemical vapor deposition (CVD)	Depends on the type of CVD reactor used, temperature gradient	Ability to individually vary reactant partial pressures allows control over relative concentration of gas phase species, deposition time controls film thickness, wafer-scale	Challenging to determine exactly when layer growth is complete due to variable incubation times, elements from precursor molecule ligands can be incorporated into films
Micromechanical assembly	In air, inert atmosphere or vacuum, assembly takes place at room temperature or with low heat to remove adhesive layers	Automated assembly platforms provide consistent and repeatable assembly of individual layers into heterostructures or devices, recent advances have approached wafer-scale assembly, ability to control relative rotation angle between layers.	Extremely sensitive to source of constituent layers, which require other synthesis techniques to make, multiple processing steps increase chances of inter-layer contaminants
Molecular beam epitaxy (MBE)	Deposition takes place at < 10 ⁻⁸ Torr, Substrate heated to increase surface diffusion rates.	In-situ characterization, layer-by-layer growth modes possible, produces epitaxial films, deposition time controls film thickness, wafer-scale	Requires epitaxial lattice match between substrate and desired material (VDWE is an exception), extremely challenging to deposit heterostructures or films with multiple constituents due to the difference in synthesis conditions
Modulated elemental reactants (MER)	Deposition takes place at < 10 ⁻⁷ Torr, annealing to self-assembly precursors typically occurs at T < ~650 °C,	Allows access to metastable compounds and heterostructures not accessible via other techniques, deposition time controls film thickness, wafer-scale	Produces films with turbostratic disorder, high grain boundary density

There are no conflicts to declare.

Author Contributions

Both authors contributed equally to this manuscript.

Conflicts of interest

Acknowledgements

DCJ acknowledges a research Humboldt Research Award from the Alexander von Humboldt Foundation. This work was

partially supported by the U.S. Department of Energy (DOE), Office of Science, Basic Energy Sciences (BES) under Award #DE-SC0020095.

References

- W. Heisenberg, *Zeitschrift für Phys.*, 1927, **43**, 172–198.
- von E. Schrödinger, *Ann. Phys.*, 1926, **384**, 361–376.
- M. M. Waldrop, *Nature*, 2016, **530**, 144–147.
- K. S. Novoselov, A. K. Geim, S. V. Morozov, D. Jiang, Y. Zhang, S. V. Dubonos, I. V. Grigorieva and A. A. Firsov, *Science (80-)*, 2004, **5**, 1–12.
- B. Partoens and F. M. Peeters, *Phys. Rev. B - Condens. Matter Mater. Phys.*, 2006, **74**, 1–11.
- P. Chandrasekhar, in *Conducting Polymers, Fundamentals and Applications*, Springer, Cham, 2018, pp. 175–249.
- A. E. Mag-Isa, J. H. Kim, H. J. Lee and C. S. Oh, *2D Mater.*, DOI:10.1088/2053-1583/2/3/034017.
- P. Blake, E. W. Hill, A. H. Castro Neto, K. S. Novoselov, D. Jiang, R. Yang, T. J. Booth and A. K. Geim, *Appl. Phys. Lett.*, DOI:10.1063/1.2768624.
- W. Li, L. Kong, C. Chen, J. Gou, S. Sheng, W. Zhang, H. Li, L. Chen, P. Cheng and K. Wu, *Sci. Bull.*, 2018, **63**, 282–286.
- F. F. Zhu, W. J. Chen, Y. Xu, C. L. Gao, D. D. Guan, C. H. Liu, D. Qian, S. C. Zhang and J. F. Jia, *Nat. Mater.*, 2015, **14**, 1020–1025.
- L. M. Schneider, S. Lippert, D. Renaud, J. Kuhnert, K. N. Kang, O. Ajayi, M. U. Halbach, O. M. Abdulmunem, X. Lin, K. Hassoon, S. Edalati-Boostan, Y. D. Kim, W. Heimbrot, E. H. Yang, J. C. Hone and A. Rahimi-Iman, *2D Mater.*, 2017, **4**, 025045.
- H. M. Dong, Z. H. Tao, L. L. Li, F. Huang, W. Xu and F. M. Peeters, *Appl. Phys. Lett.*, DOI:10.1063/5.0006617.
- S. Park, T. Schultz, X. Xu, B. Wegner, A. Aljarb, A. Han, L. J. Li, V. C. Tung, P. Amsalem and N. Koch, *Commun. Phys.*, DOI:10.1038/s42005-019-0212-y.
- L. Li, S. Z. Lu, J. Pan, Z. Qin, Y. Q. Wang, Y. Wang, G. Y. Cao, S. Du and H. J. Gao, *Adv. Mater.*, 2014, **26**, 4820–4824.
- J. L. Zhang, S. Zhao, C. Han, Z. Wang, S. Zhong, S. Sun, R. Guo, X. Zhou, C. D. Gu, K. Di Yuan, Z. Li and W. Chen, *Nano Lett.*, 2016, **16**, 4903–4908.
- C. Brosseau and A. Beroual, *Prog. Mater. Sci.*, 2003, **48**, 373–456.
- S. Schulz and G. Czycholl, *Phys. Rev. B - Condens. Matter Mater. Phys.*, 2005, **72**, 1–13.
- G. Bester, *J. Phys. Condens. Matter*, DOI:10.1088/0953-8984/21/2/023202.
- X. Zhang, K. H. Jin, J. Mao, M. Zhao, Z. Liu and F. Liu, *npj Comput. Mater.*, 2021, **7**, 1–8.
- L. Kou, S. C. Wu, C. Felser, T. Frauenheim, C. Chen and B. Yan, *ACS Nano*, 2014, **8**, 10448–10454.
- U. Dey, M. Chakraborty, A. Taraphder and S. Tewari, *Sci. Rep.*, 2018, **8**, 1–11.
- M. R. Rosenberger, H. J. Chuang, K. M. McCreary, A. T. Hanbicki, S. V. Sivaram and B. T. Jonker, *ACS Appl. Mater. Interfaces*, 2018, **10**, 10379–10387.
- H. W. Guo, Z. Hu, Z. B. Liu and J. G. Tian, *Adv. Funct. Mater.*, 2021, **31**, 1–32.
- Y. Huang, Y. H. Pan, R. Yang, L. H. Bao, L. Meng, H. L. Luo, Y. Q. Cai, G. D. Liu, W. J. Zhao, Z. Zhou, L. M. Wu, Z. L. Zhu, M. Huang, L. W. Liu, L. Liu, P. Cheng, K. H. Wu, S. B. Tian, C. Z. Gu, Y. G. Shi, Y. F. Guo, Z. G. Cheng, J. P. Hu, L. Zhao, G. H. Yang, E. Sutter, P. Sutter, Y. L. Wang, W. Ji, X. J. Zhou and H. J. Gao, *Nat. Commun.*, DOI:10.1038/s41467-020-16266-w.
- C. H. Lee, G. H. Lee, A. M. Van Der Zande, W. Chen, Y. Li, M. Han, X. Cui, G. Arefe, C. Nuckolls, T. F. Heinz, J. Guo, J. Hone and P. Kim, *Nat. Nanotechnol.*, 2014, **9**, 676–681.
- S. Natarajan, M. Agostinelli, S. Akbar, M. Bost, A. Bowonder, V. Chikarmane, S. Chouksey, A. Dasgupta, K. Fischer, Q. Fu, T. Ghani, M. Giles, S. Govindaraju, R. Grover, W. Han, D. Hanken, E. Haralson, M. Haran, M. Heckscher, R. Heussner, P. Jain, R. James, R. Jhaveri, I. Jin, H. Kam, E. Karl, C. Kenyon, M. Liu, Y. Luo, R. Mehandru, S. Morarka, L. Neiberg, P. Packan, A. Paliwal, C. Parker, P. Patel, R. Patel, C. Pelto, L. Pipes, P. Plekhanov, M. Prince, S. Rajamani, J. Sandford, B. Sell, S. Sivakumar, P. Smith, B. Song, K. Tone, T. Troeger, J. Wiedemer, M. Yang and K. Zhang, in *2014 IEEE International Electron Devices Meeting*, 2014, pp. 3.7.1-3.7.3.
- K. S. Novoselov, A. Mishchenko, A. Carvalho and A. H. Castro Neto, *Science (80-)*, DOI:10.1126/science.aac9439.
- K. S. Novoselov, S. V. Morozov, T. M. G. Mohinddin, L. A. Ponomarenko, D. C. Elias, R. Yang, I. I. Barbolina, P. Blake, T. J. Booth, D. Jiang, J. Giesbers, E. W. Hill and A. K. Geim, *Phys. Status Solidi Basic Res.*, 2007, **244**, 4106–4111.
- E. Blundo, M. Felici, T. Yildirim, G. Pettinari, D. Tedeschi, A. Miriametro, B. Liu, W. Ma, Y. Lu and A. Polimeni, *Phys. Rev. Res.*, 2020, **2**, 1–7.
- C. Ernanandes, L. Khalil, H. Almabrouk, D. Pierucci, B. Zheng, J. Avila, P. Dudin, J. Chaste, F. Oehler, M. Pala, F. Bisti, T. Brulé, E. Lhuillier, A. Pan and A. Ouerghi, *npj 2D Mater. Appl.*, 2021, **5**, 1–7.
- Y. Sun, D. Wang and Z. Shuai, *J. Phys. Chem. C*, 2016, **120**, 21866–21870.
- M. Falmbigl, A. Fiedler, R. E. Atkins, S. F. Fischer and D. C. Johnson, *Nano Lett.*, 2015, **15**, 943–948.
- J. Feng, D. Biswas, A. Rajan, M. D. Watson, F. Mazzola, O. J. Clark, K. Underwood, I. Marković, M. McLaren, A. Hunter, D. M. Burn, L. B. Duffy, S. Barua, G. Balakrishnan, F. Bertran, P. Le Fèvre, T. K. Kim, G. Van Der Laan, T. Hesjedal, P. Wahl and P. D. C. King, *Nano Lett.*, 2018, **18**, 4493–4499.
- G. Duvjir, B. K. Choi, I. Jang, S. Ulstrup, S. Kang, T. Thi Ly, S. Kim, Y. H. Choi, C. Jozwiak, A. Bostwick, E. Rotenberg, J. G. Park, R. Sankar, K. S. Kim, J. Kim and Y. J. Chang, *Nano Lett.*, 2018, **18**, 5432–5438.
- P. Chen, W. W. Pai, Y. H. Chan, V. Madhavan, M. Y. Chou, S. K. Mo, A. V. Fedorov and T. C. Chiang, *Phys. Rev. Lett.*, 2018, **121**, 1–6.
- M. D. Anderson, C. L. Heideman, Q. Lin, M. Smeller, R. Kokenyesi, A. A. Herzing, I. M. Anderson, D. A. Keszler, P. Zschack and D. C. Johnson, *Angew. Chemie - Int. Ed.*, 2013, **52**, 1982–1985.
- A. L. Friedman, A. T. Hanbicki, F. K. Perkins, G. G. Jernigan, J. C. Culbertson and P. M. Campbell, *Sci. Rep.*, 2017, **7**, 1–9.
- M. A. Choffel, T. M. Kam and D. C. Johnson, *Inorg. Chem.*, 2021, **60**, 9598–9606.
- M. A. Choffel, R. N. Gannon, F. Göhler, A. M. Miller, D. L. Medlin, T. Seyller and D. C. Johnson, *Chem. Mater.*, 2021, **33**, 6403–6411.
- D. M. Hamann, S. R. Bauers, A. M. Miller, J. Ditto, D. B. Moore and D. C. Johnson, *Inorg. Chem.*, 2020, **59**, 10928–10937.

- 41 M. Esters, M. B. Alemayehu, Z. Jones, N. T. Nguyen, M. D. Anderson, C. Grosse, S. F. Fischer and D. C. Johnson, *Angew. Chemie - Int. Ed.*, 2015, **54**, 1130–1134.
- 42 M. Noh and D. C. Johnson, *J. Am. Chem. Soc.*, 1996, **118**, 9117–9122.
- 43 N. S. Gunning, J. Feser, M. Beekman, D. G. Cahill and D. C. Johnson, *J. Am. Chem. Soc.*, 2015, **137**, 8803–8809.
- 44 J. Rouxel, A. Meerschaut and G. A. Wiegers, *J. Alloys Compd.*, 1995, **229**, 144–157.
- 45 G. A. Wiegers and A. Meerschaut, *Mater. Sci. Forum*, 1992, **100–101**, 101–172.
- 46 K. Kato, I. Kawada and T. Takahashi, *Acta Crystallogr. Sect. B Struct. Crystallogr. Cryst. Chem.*, 1977, **33**, 3437–3443.
- 47 J. R. Chamorro and T. M. McQueen, *Acc. Chem. Res.*, 2018, **51**, 2918–2925.
- 48 A. Jain, S. P. Ong, G. Hautier, W. Chen, W. D. Richards, S. Dacek, S. Cholia, D. Gunter, D. Skinner, G. Ceder and K. A. Persson, *APL Mater.*, 2013, **1**, 1–11.
- 49 J. J. de Pablo, N. E. Jackson, M. A. Webb, L. Q. Chen, J. E. Moore, D. Morgan, R. Jacobs, T. Pollock, D. G. Schlom, E. S. Toberer, J. Analytis, I. Dabo, D. M. DeLongchamp, G. A. Fiete, G. M. Grason, G. Hautier, Y. Mo, K. Rajan, E. J. Reed, E. Rodriguez, V. Stevanovic, J. Suntivich, K. Thornton and J. C. Zhao, *npj Comput. Mater.*, 2019, **5**, 1–23.
- 50 K. Kovnir, *Chem. Mater.*, 2021, **33**, 4835–4841.
- 51 N. Giang, Q. Xu, Y. S. Hor, A. J. Williams, S. E. Dutton, H. W. Zandbergen and R. J. Cava, *Phys. Rev. B - Condens. Matter Mater. Phys.*, 2010, **82**, 1–5.
- 52 A. M. Miller, D. M. Hamann, E. C. Hadland and D. C. Johnson, *Inorg. Chem.*, 2020, **59**, 12536–12544.
- 53 P. G. Vekilov, *Cryst. Growth Des.*, 2010, **10**, 5007–5019.
- 54 K. A. Jackson, *Ind. Eng. Chem.*, 1965, **57**, 28–32.
- 55 E. Mura and Y. Ding, *Adv. Colloid Interface Sci.*, 2021, **289**, 102361.
- 56 J. Q. Geisenhoff, A. K. Tamura and A. M. Schimpf, *Chem. Commun.*, 2019, **55**, 8856–8859.
- 57 M. S. Sokolikova, P. C. Sherrell, P. Palczynski, V. L. Bemmer and C. Mattevi, *Nat. Commun.*, DOI:10.1038/s41467-019-08594-3.
- 58 J. H. Perepezko, *Prog. Mater. Sci.*, 2004, **49**, 263–284.
- 59 D. J. Kelly, N. Clark, M. Zhou, D. Gebauer, R. V. Gorbachev and S. J. Haigh, *Adv. Mater.*, DOI:10.1002/adma.202100668.
- 60 M. Moliner, Y. Román-Leshkov and A. Corma, *Acc. Chem. Res.*, 2019, **52**, 2971–2980.
- 61 M. G. Kanatzidis, *Acc. Chem. Res.*, 2005, **38**, 359–368.
- 62 D. Wang, F. Luo, M. Lu, X. Xie, L. Huang and W. Huang, *Small*, 2019, **15**, 1–12.
- 63 R. P. Sear, *J. Phys. Condens. Matter*, DOI:10.1088/0953-8984/19/3/033101.
- 64 D. Hu, G. Xu, L. Xing, X. Yan, J. Wang, J. Zheng, Z. Lu, P. Wang, X. Pan and L. Jiao, *Angew. Chemie - Int. Ed.*, 2017, **56**, 3611–3615.
- 65 M. Binnewies, R. Glaum, M. Schmidt and P. Schmidt, *Chem. Vap. Transp. React.*, DOI:10.1515/9783110254655.
- 66 J. You, M. D. Hossain and Z. Luo, *Nano Converg.*, DOI:10.1186/s40580-018-0158-x.
- 67 N. Briggs, S. Subramanian, Z. Lin, X. Li, X. Zhang, K. Zhang, K. Xiao, D. Geohagan, R. Wallace, L. Q. Chen, M. Terrones, A. Ebrahimi, S. Das, J. Redwing, C. Hinkle, K. Momeni, A. Van Duin, V. Crespi, S. Kar and J. A. Robinson, *2D Mater.*, DOI:10.1088/2053-1583/aaf836.
- 68 W. M. Haynes, Ed., *CRC Handbook of Chemistry and Physics*, CRC Press, 2014.
- 69 Y. Kajikawa and S. Noda, *Appl. Surf. Sci.*, 2005, **245**, 281–289.
- 70 Z. Cai, B. Liu, X. Zou and H. M. Cheng, *Chem. Rev.*, 2018, **118**, 6091–6133.
- 71 F. J. J. Di Salvo, D. E. E. Moncton and J. V. V. Waszczak, *Phys. Rev. B*, 1976, **14**, 4321–4328.
- 72 K. A. Lozovoy, A. G. Korotaev, A. P. Kokhanenko, V. V. Dirko and A. V. Voitsekhovskii, *Surf. Coatings Technol.*, 2020, **384**, 125289.
- 73 B. Daudin, F. Widmann, G. Feuillet, Y. Samson, M. Arlery and J. Rouvière, *Phys. Rev. B - Condens. Matter Mater. Phys.*, 1997, **56**, R7069–R7072.
- 74 Y. Kajikawa, T. Tsuchiya, S. Noda and H. Komiyama, *Chem. Vap. Depos.*, 2004, **10**, 128–133.
- 75 F. C. Frank and J. H. van der Merwe, *Proc. R. Soc. A Math. Phys. Eng. Sci.*, 1949, **198**, 216–225.
- 76 M. Volmer and A. Weber, *Zeitschrift für Phys. Chemie*, 1926, **119U**, 277–301.
- 77 I. N. Stranski and L. Krastanow, *Monatshefte für Chemie*, 1939, **72**, 76.
- 78 W. Zheng, B. Zheng, C. Yan, Y. Liu, X. Sun, Z. Qi, T. Yang, Y. Jiang, W. Huang, P. Fan, F. Jiang, W. Ji, X. Wang and A. Pan, *Adv. Sci.*, DOI:10.1002/advs.201802204.
- 79 C. R. Dean, A. F. Young, I. Meric, C. Lee, L. Wang, S. Sorgenfrei, K. Watanabe, T. Taniguchi, P. Kim, K. L. Shepard and J. Hone, *Nat. Nanotechnol.*, 2010, **5**, 722–726.
- 80 X. Cao, C. Jiang, D. Tan, Q. Li, S. Bi and J. Song, *J. Sci. Adv. Mater. Devices*, 2021, **6**, 135–152.
- 81 Z. Hu, Z. B. Liu and J. G. Tian, *Chinese J. Chem.*, 2020, **38**, 981–995.
- 82 S. Wang, X. Cui, C. Jian, H. Cheng, M. Niu, J. Yu, J. Yan and W. Huang, *Adv. Mater.*, 2021, **33**, 1–21.
- 83 M. Seol, M. H. Lee, H. Kim, K. W. Shin, Y. Cho, I. Jeon, M. Jeong, H. I. Lee, J. Park and H. J. Shin, *Adv. Mater.*, 2020, **32**, 1–8.
- 84 H. Park, J. Kang, M. Kim, J. Seo, J. Kim, J. S. Moon, J. Lee and J. H. Kim, *ACS Nano*, 2021, **15**, 3038–3046.
- 85 R. F. Frindt, *Phys. Rev. Lett.*, 1972, **28**, 299–301.
- 86 J. N. Coleman, M. Lotya, A. O'Neill, S. D. Bergin, P. J. King, U. Khan, K. Young, A. Gaucher, S. De, R. J. Smith, I. V. Shvets, S. K. Arora, G. Stanton, H. Y. Kim, K. Lee, G. T. Kim, G. S. Duesberg, T. Hallam, J. J. Boland, J. J. Wang, J. F. Donegan, J. C. Grunlan, G. Moriarty, A. Shmeliov, R. J. Nicholls, J. M. Perkins, E. M. Grieveson, K. Theuvsissen, D. W. McComb, P. D. Nellist and V. Nicolosi, *Science (80-.)*, 2011, **331**, 568–571.
- 87 X. Fan, P. Xu, D. Zhou, Y. Sun, Y. C. Li, M. A. T. Nguyen, M. Terrones and T. E. Mallouk, *Nano Lett.*, 2015, **15**, 5956–5960.
- 88 D. Sangian, Y. Ide, Y. Bando, A. E. Rowan and Y. Yamauchi, *Small*, 2018, **14**, 1–14.
- 89 K. Kang, K. H. Lee, Y. Han, H. Gao, S. Xie, D. A. Muller and J. Park, *Nature*, 2017, **550**, 229–233.
- 90 S. B. Desai, S. R. Madhupathy, M. Amani, D. Kiriya, M. Hettick, M. Tosun, Y. Zhou, M. Dubey, J. W. Ager, D. Chrzan and A. Javey, *Adv. Mater.*, 2016, **28**, 4053–4058.
- 91 G. Z. Magda, J. Pető, G. Dobrik, C. Hwang, L. P. Biró and L. Tapasztó, *Sci. Rep.*, 2015, **5**, 3–7.
- 92 M. Velický, G. E. Donnelly, W. R. Hendren, S. McFarland, D. Scullion, W. J. I. DeBenedetti, G. C. Correa, Y. Han, A. J.

- Wain, M. A. Hines, D. A. Muller, K. S. Novoselov, H. D. Abruña, R. M. Bowman, E. J. G. Santos and F. Huang, *ACS Nano*, 2018, **12**, 10463–10472.
- 93 Y. Cao, V. Fatemi, S. Fang, K. Watanabe, T. Taniguchi, E. Kaxiras and P. Jarillo-Herrero, *Nature*, 2018, **556**, 43–50.
- 94 S. J. Yang, J. H. Jung, E. Lee, E. Han, M. Y. Choi, D. Jung, S. Choi, J. H. Park, D. Oh, S. Noh, K. J. Kim, P. Y. Huang, C. C. Hwang and C. J. Kim, *Nano Lett.*, 2021, 1–7.
- 95 K. Kang, K. H. Lee, Y. Han, H. Gao, S. Xie, D. A. Muller and J. Park, *Nature*, 2017, **550**, 229–233.
- 96 L. A. Walsh and C. L. Hinkle, *Appl. Mater. Today*, 2017, **9**, 504–515.
- 97 C. W. Liu, J. J. Dai, S. K. Wu, N. Q. Diep, S. H. Huynh, T. T. Mai, H. C. Wen, C. T. Yuan, W. C. Chou, J. L. Shen and H. H. Luc, *Sci. Rep.*, 2020, **10**, 1–8.
- 98 P. Sheldon, K. M. Jones, M. M. Al-Jassim and B. G. Yacobi, *J. Appl. Phys.*, 1988, **63**, 5609–5611.
- 99 K. Mohammed, D. A. Cammack, R. Dalby, P. Newbury, B. L. Greenberg, J. Petruzzello and R. N. Bhargava, *Appl. Phys. Lett.*, 1987, **50**, 37–39.
- 100 B. Harold, in *Surface and Interface Science, Volume 4: Solid-Solid Interfaces and Thin Films*, ed. K. Wandelt, Wiley-VCH Verlag, 1st edn., 2014.
- 101 K. Ismail, *J. Vac. Sci. Technol. B Microelectron. Nanom. Struct.*, 1996, **14**, 2776.
- 102 A. Koma and K. Yoshimura, *Surf. Sci.*, 1986, **174**, 556–560.
- 103 A. Koma, K. Sunouchi and T. Miyajima, *Microelectron. Eng.*, 1984, **2**, 129–136.
- 104 K. Ueno, T. Shimada, K. Saiki and A. Koma, *Appl. Phys. Lett.*, 1990, **56**, 327–329.
- 105 S. G. Liu, S. N. Subbarao, A. Rosen, D. Sarnoff and C. H. Lee, *Microw. Opt. Technol. Lett.*, 1993, **6**, 32–33.
- 106 A. Koma, K. Saiki and Y. Sato, *Appl. Surf. Sci.*, 1989, **42**, 451–456.
- 107 K. Ueno, K. Sasaki, K. Saiki and A. Koma, *Japanese J. Appl. Physics, Part 1 Regul. Pap. Short Notes Rev. Pap.*, 1999, **38**, 511–514.
- 108 T. Löher, Y. Tomm, A. Klein, D. Su, C. Pettenkofer and W. Jaegermann, *J. Appl. Phys.*, 1996, **80**, 5718–5722.
- 109 R. Schlaf, C. Pettenkofer and W. Jaegermann, *J. Appl. Phys.*, 1999, **85**, 6550–6556.
- 110 M. Iqbal, B. Utama, Z. Peng, R. Chen, B. Peng, X. Xu, Y. Dong, M. Wong, S. Wang, H. Sun and Q. Xiong, *Nano Lett.*, 2011, **11**, 3051–3057.
- 111 Y. L. Chen, J. G. Analytis, J.-H. Chu, Z. K. Liu, S.-K. Mo, X. L. Qi, H. J. Zhang, D. H. Lu, X. Dai, Z. Fang, S. C. Zhang, I. R. Fisher, Z. Hussain and Z.-X. Shen, *Science (80-.)*, 2009, **325**, 178–181.
- 112 H. C. Diaz, R. Chaghi, Y. Ma and M. Batzill, *2D Mater.*, DOI:10.1088/2053-1583/2/4/044010.
- 113 H. C. Diaz, Y. Ma, S. Kolekar, J. Avila, C. Chen, M. C. Asensio and M. Batzill, *2D Mater.*, DOI:10.1088/2053-1583/aa6e6a.
- 114 R. Yue, Y. Nie, L. A. Walsh, R. Addou, C. Liang, N. Lu, A. T. Barton, H. Zhu, Z. Che, D. Barrera, L. Cheng, P. R. Cha, Y. J. Chabal, J. W. P. Hsu, J. Kim, M. J. Kim, L. Colombo, R. M. Wallace, K. Cho and C. L. Hinkle, *2D Mater.*, DOI:10.1088/2053-1583/aa8ab5.
- 115 B. A. Joyce, D. D. Vvedensky, G. R. Bell, J. G. Belk, M. Itoh and T. S. Jones, *Mater. Sci. Eng. B Solid-State Mater. Adv. Technol.*, 1999, **67**, 7–16.
- 116 T. Hotta, T. Tokuda, S. Zhao, K. Watanabe, T. Taniguchi, H. Shinohara and R. Kitaura, *Appl. Phys. Lett.*, DOI:10.1063/1.4963178.
- 117 L. Jiao, The University of Hong Kong, 2015.
- 118 D. L. Partin, C. M. Thrush, S. J. Simko and S. W. Gaarenstroom, *J. Appl. Phys.*, 1989, **66**, 6115–6120.
- 119 L. A. Walsh, R. Yue, Q. Wang, A. T. Barton, R. Addou, C. M. Smyth, H. Zhu, J. Kim, L. Colombo, M. J. Kim, R. M. Wallace and C. L. Hinkle, *2D Mater.*, DOI:10.1088/2053-1583/aa61e1.
- 120 H. Liu and Y. Xue, *Adv. Mater.*, 2021, **2008456**, 2–9.
- 121 S. Chen, H. Liu, F. Chen, K. Zhou and Y. Xue, *ACS Nano*, 2020, **14**, 11473–11481.
- 122 X. Sun, W. Li, X. Wang, Q. Sui, T. Zhang, Z. Wang, L. Liu, D. Li, S. Feng, S. Zhong, H. Wang, V. Bouchiat, M. Nunez Regueiro, N. Rougemaille, J. Coraux, A. Purbawati, A. Hadj-Azzem, Z. Wang, B. Dong, X. Wu, T. Yang, G. Yu, B. Wang, Z. Han, X. Han and Z. Zhang, *Nano Res.*, 2020, **13**, 3358–3363.
- 123 B. Li, Z. Wan, C. Wang, P. Chen, B. Huang, X. Cheng, Q. Qian, J. Li, Z. Zhang, G. Sun, B. Zhao, H. Ma, R. Wu, Z. Wei, Y. Liu, L. Liao, Y. Ye, Y. Huang, X. Xu, X. Duan, W. Ji and X. Duan, *Nat. Mater.*, 2021, **20**, 818–825.
- 124 M. Kan, S. Adhikari and Q. Sun, *Phys. Chem. Chem. Phys.*, 2014, **16**, 4990–4994.
- 125 M. Aykol, S. S. Dwaraknath, W. Sun and K. A. Persson, *Sci. Adv.*, 2018, **4**, 1–8.
- 126 R. B. Schwarz and W. L. Johnson, *Phys. Rev. Lett.*, 1983, **51**, 415–418.
- 127 E. J. Cotts, W. J. Meng and W. L. Johnson, *Phys. Rev. Lett.*, 1986, **57**, 2295.
- 128 R. B. Schwarz, K. L. Wong, W. L. Johnson and B. M. Clemens, *J. Non. Cryst. Solids*, 1984, **61–62**, 129–134.
- 129 T. Novet, J. M. McConnell and D. C. Johnson, *Chem. Mater.*, 1992, **4**, 473–478.
- 130 L. Fister and D. C. Johnson, *J. Am. Chem. Soc.*, 1992, **114**, 4639–4644.
- 131 M. Fukuto, M. D. Hornbostel and D. C. Johnson, *J. Am. Chem. Soc.*, 1994, **116**, 9136–9140.
- 132 T. Novet and D. C. Johnson, *J. Am. Chem. Soc.*, 1991, **113**, 3398–3403.
- 133 J. R. Williams, M. Johnson and D. C. Johnson, *J. Am. Chem. Soc.*, 2001, **123**, 1645–1649.
- 134 M. D. Hornbostel, E. J. Hyer, J. Thiel and D. C. Johnson, *J. Am. Chem. Soc.*, 1997, **119**, 2665–2668.
- 135 N. Pienack and W. Bensch, *Angew. Chemie - Int. Ed.*, 2011, **50**, 2014–2034.
- 136 M. Regus, S. Mankovsky, S. Polesya, G. Kuhn, J. Ditto, U. Schürmann, A. Jacquot, K. Bartholomé, C. Näther, M. Winkler, J. D. König, H. Böttner, L. Kienle, D. C. Johnson, H. Ebert and W. Bensch, *J. Solid State Chem.*, 2015, **230**, 254–265.
- 137 M. Jansen, *Angew. Chemie - Int. Ed.*, 2002, **41**, 3746–3766.
- 138 D. Fischer and M. Jansen, *J. Am. Chem. Soc.*, 2002, **124**, 3488–3489.
- 139 D. Fischer, A. Müller and M. Jansen, *Zeitschrift für Anorg. und Allg. Chemie*, 2004, **630**, 2697–2700.
- 140 D. Fischer and M. Jansen, *Angew. Chemie - Int. Ed.*, 2002, **41**, 1755–1756.
- 141 D. C. Johnson, *Curr. Opin. Solid State Mater. Sci.*, 1998, **3**, 159–167.
- 142 M. Noh, J. Thiel and D. C. Johnson, *Science (80-.)*, 1995, **270**, 1181–1184.
- 143 M. Beekman, S. Disch, S. Rouvimov, D. Kasinathan, K.

- Koepernik, H. Rosner, P. Zschack, W. S. Neumann and D. C. Johnson, *Angew. Chemie - Int. Ed.*, 2013, **52**, 13211–13214.
- 144 D. L. Mesoza Cordova, T. M. Kam, R. N. Gannon, P. Lu and D. C. Johnson, *J. Am. Chem. Soc.*, 2020, **142**, 13145–13154.
- 145 O. Oyelaran, T. Novet, C. D. Johnson and D. C. Johnson, *J. Am. Chem. Soc.*, 1996, **118**, 2422–2426.
- 146 J. R. Williams, M. B. Johnson and D. C. Johnson, *J. Am. Chem. Soc.*, 2003, **125**, 3589–3592.
- 147 M. D. Anderson, J. O. Thompson and D. C. Johnson, *Chem. Mater.*, 2013, **25**, 3996–4002.
- 148 M. Overbay, T. Novet and D. C. Johnson, *J. Solid State Chem.*, 1996, **123**, 337–343.
- 149 D. R. Merrill, D. B. Moore, J. Ditto, D. R. Sutherland, M. Falmbigl, M. Winkler, H. F. Pernau and D. C. Johnson, *Eur. J. Inorg. Chem.*, 2015, **2015**, 83–91.
- 150 D. M. Hamann, D. Bardgett, S. R. Bauers, T. W. Kasel, A. M. Mroz, C. H. Hendon, D. L. Medlin and D. C. Johnson, *Chem. Mater.*, 2020, **32**, 5802–5813.
- 151 D. M. Hamann, A. C. Lygo, M. Esters, D. R. Merrill, J. Ditto, D. R. Sutherland, S. R. Bauers and D. C. Johnson, *ACS Nano*, 2018, acsnano.7b07506.
- 152 D. R. Merrill, D. R. Sutherland, D. B. Moore, M. Falmbigl, L. Medlin and D. C. Johnson, *Nanoscale*, 2016, **8**, 13646–13651.
- 153 F. R. Harris, S. Standridge and D. C. Johnson, *J. Am. Chem. Soc.*, 2005, **127**, 7843–7848.
- 154 F. R. Harris, S. Standridge, C. Feik and D. C. Johnson, *Angew. Chemie - Int. Ed.*, 2003, **42**, 5296–5299.
- 155 C. L. Heideman, S. Tepfer, Q. Lin, R. Rostek, P. Zschack, M. D. Anderson, I. M. Anderson and D. C. Johnson, *J. Am. Chem. Soc.*, 2013, **135**, 11055–11062.
- 156 E. Hadland, H. Jang, M. Falmbigl, R. Fischer, D. L. Medlin, D. G. Cahill and D. C. Johnson, *Chem. Mater.*, 2019, **31**, 5699–5705.
- 157 Q. Lin, M. Smeller, C. L. Heideman, P. Zschack, M. Koyano, M. D. Anderson, R. Kykyneshi, D. A. Keszler, I. M. Anderson and D. C. Johnson, *Chem. Mater.*, 2010, **22**, 1002–1009.
- 158 Q. Lin, S. Tepfer, C. Heideman, C. Mortensen, N. Nguyen, P. Zschack, M. Beekman and D. C. Johnson, *J. Mater. Res.*, 2011, **26**, 1866–1871.
- 159 D. B. Moore, M. Beekman, S. Disch and D. C. Johnson, *Angew. Chemie*, 2014, **126**, 5778–5781.
- 160 D. Bardgett, R. N. Gannon, D. M. Hamann, D. M. Roberts, S. R. Bauers, P. Lu and D. C. Johnson, *Chem. Mater.*, 2021, **33**, 2585–2592.
- 161 A. C. Lygo, D. M. Hamann, D. B. Moore, D. R. Merrill, J. Ditto, M. Esters, J. Orłowicz, S. R. Wood and D. C. Johnson, *J. Am. Chem. Soc.*, 2018, **140**, 3385–3393.
- 162 N. S. Gunning, T. Dankwort, M. Falmbigl, U. Ross, G. Mitchson, D. M. Hamann, A. Lotnyk, L. Kienle and D. C. Johnson, *Chem. Mater.*, 2017, **29**, 8292–8298.
- 163 Z. Xu, Z. Tang, S. D. Kevan, T. Novet and D. C. Johnson, *J. Appl. Phys.*, 1993, **74**, 905–912.
- 164 T. Novet, S. Kevan and D. C. Johnson, *Mater. Sci. Eng. A*, 1995, **195**, 21–27.
- 165 T. Phung, J. Jensen, D. Jonshon, J. Donovan and B. McBurnett, *X-Ray Spectrom.*, 2008, **37**, 608–614.
- 166 D. M. Hamann, D. Bardgett, D. L. M. Cordova, L. A. Maynard, E. C. Hadland, A. C. Lygo, S. R. Wood, M. Esters and D. C. Johnson, *Chem. Mater.*, 2018, **30**, 6209–6216.
- 167 S. R. Bauers, S. R. Wood, K. M. Ø. Jensen, A. B. Blichfeld, B. B. Iversen, S. J. L. Billinge and D. C. Johnson, *J. Am. Chem. Soc.*, 2015, **137**, 9652–9658.
- 168 J. Ditto, D. R. Merrill, G. Mitchson, J. J. Gabriel, K. Mathew, R. G. Hennig, D. L. Medlin, N. D. Browning and D. C. Johnson, *Angew. Chemie - Int. Ed.*, 2017, **56**, 14448–14452.
- 169 M. Jansen, *Pure Appl. Chem.*, 2014, **86**, 883–898.
- 170 M. Jansen and J. C. Schön, *Angew. Chemie - Int. Ed.*, 2006, **45**, 3406–3412.
- 171 W. Y. Zhou, A. Meetsma, J. L. de Boer and G. A. Wiegers, *Mater. Res. Bull.*, 1992, **27**, 563–572.
- 172 N. Bassim, K. Scott and L. A. Giannuzzi, *MRS Bull.*, 2014, **39**, 317–325.
- 173 R. R. Schröder, *Arch. Biochem. Biophys.*, 2015, **581**, 25–38.
- 174 G. Guzzinati, T. Altantzis, M. Batuk, A. De Backer, G. Lumbeeck, V. Samaee, D. Batuk, H. Idrissi, J. Hadermann, S. Van Aert, D. Schryvers, J. Verbeeck and S. Bals, *Materials (Basel)*, , DOI:10.3390/ma11081304.
- 175 D. J. Stokes, *Philos. Trans. R. Soc. A Math. Phys. Eng. Sci.*, 2003, **361**, 2771–2787.
- 176 *Nat. Methods*, 2016, **13**, 1.